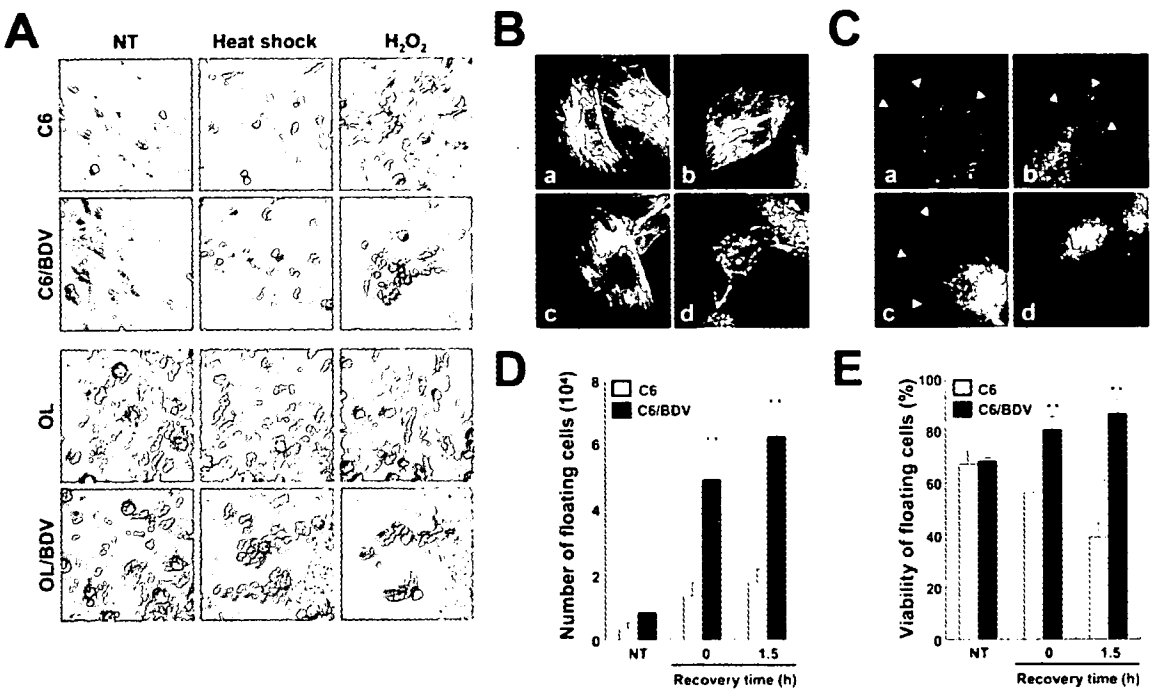

FIG. 3. Suppression of the thermotolerance of persistently infected cell lines. (A) Morphological changes of BDV-infected glial cells. Cells were exposed to heat stress at 44°C for 1 h or to oxidative stress with 10 μM hydrogen peroxide for 0.5 h. In the case of oxidative stress, cells were allowed to recover for 24 h in normal medium at 37°C. For morphological analysis, cells were visualized under a phase-contrast microscope. (B and C) Disruption of the actin cytoskeleton and focal adhesion complexes in persistently BDV-infected C6 cells. C6 cells were exposed to heat stress at 44°C for 1 h. Subpanels: a and b, uninfected; c and d, persistently infected. Stress-treated (b and d) and untreated (a and c) cells were fixed and stained with rhodamine-phalloidin (B) or anti-FAK antibody (C). Arrowheads indicate FAK at the lamellipodia. (D) After heat stress, cells were recovered at 37°C. The floating cells in the culture supernatants were counted at 0 and 1.5 h of recovery. (E) The floating cells were stained with 0.4% trypan blue, and the viable cells were counted. The data are expressed as percentages of the total number of cells counted. For statistical analysis, the data were expressed as the mean plus the standard error. Comparisons of two groups were performed by Student's *t* test with the Statcel software. Double asterisks indicate statistically significant differences ($P < 0.01$). NT, nontreated control cells.

stress of 44°C for 1 h and analyzed HSP70 expression, as well as morphological alteration. As shown in Fig. 4B, uninfected primary cells showed significant upregulation of HSP70 from 3 h after heat stress. In contrast, reduced activation of HSP70 was found only from 6 h after treatment in BDV-infected primary glial cells. Furthermore, morphological changes, such as rounding and flatten and shape forms, were observed only in BDV-infected cells within 1 h after treatment (Fig. 4D). This experiment suggested the possibility that altered expression of HSP70 may occur in persistently BDV-infected glial cells even in infected brains.

BDV causes instability of HSP70 mRNA and PKR activation in persistently infected cells. Previous studies revealed that expression of heat shock genes is regulated at both the transcriptional and posttranscriptional levels (21, 27). Thus, we next examined the time course of the expression of HSP70 mRNA in C6/BDV cells after heat shock followed by 12 h of recovery at 37°C. As shown in Fig. 5A, HSP70 mRNA expression was rapidly induced by heat shock in both infected and uninfected cells, suggesting that HSP70 mRNA transcription was not affected by BDV persistence. However, interestingly, HSP70 mRNA expression completely disappeared in persistently infected cells by 6 h after heat shock (Fig. 5A). The levels of expression of housekeeping gene and BDV N and P mRNAs were similar in uninfected and infected C6 cells with or without heat shock, indicating a relatively specific effect of heat on HSP70 mRNA expression. To confirm the instability of HSP70 mRNA in persistently BDV-infected cells, we determined the relative stability of HSP70 mRNA in stress-treated cells. BDV-infected and uninfected C6 cells were heat shocked at 44°C and then allowed to recover at 37°C in the presence of actinomycin D for 12 h. Actinomycin D blocks the de novo synthesis of most mRNAs at the transcriptional level, and therefore kinetic changes in cellular mRNA could reflect the relative degree of turnover. As shown in Fig. 5C, HSP70 mRNA was relatively stable in heat-shocked uninfected C6 cells, and its half-life was estimated as 9 h after heat stress (Fig. 5C). On the other hand, in persistently BDV-infected cells, the level of HSP70 mRNA declined by 50% within the 4-h incubation period (Fig. 5C). These results suggested that BDV persistence is involved in the posttranscriptional stabilization of HSP70 mRNA.

A recent paper has reported that stress-induced PKR stabilizes HSP70 mRNA through interaction with the AU-rich elements present in the 3′ untranslated region of the HSP70 mRNA (55). On the other hand, it has also been demonstrated that induction of HSP70 directly plays a role in the suppression of PKR upregulation (25, 33, 34). These studies indicate that

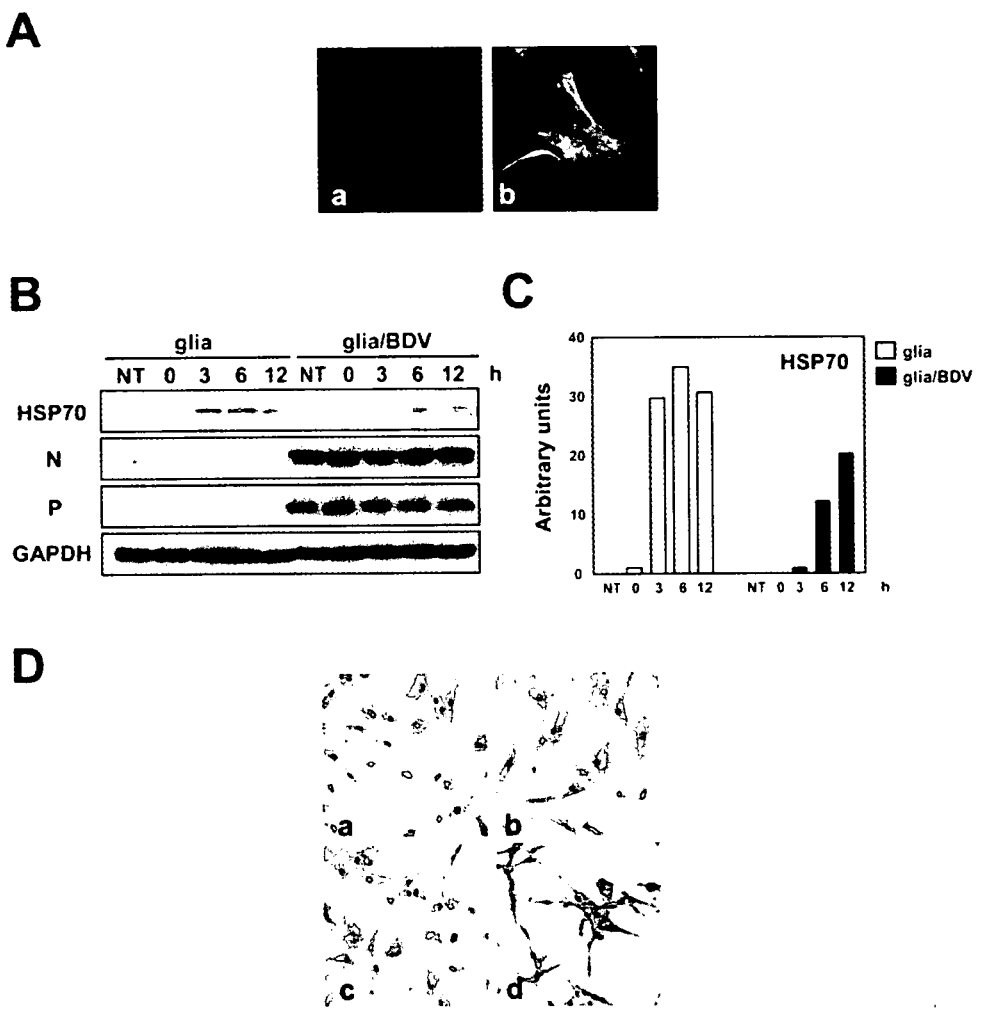

FIG. 4. Effects of BDV infection on HSP70 induction in primary glial cells. (A) Primary glial cells were isolated and infected with BDV as described in Materials and Methods. BDV antigen was detected by immunofluorescence assay with an anti-P polyclonal antibody. Subpanels: a, uninfected; b, BDV infected. (B) Primary glial cells were exposed to heat shock at 44°C and allowed to recover at 37°C for different times. Cells were harvested at the indicated times in the recovery period. Nontreated control cells (NT) were maintained at 37°C and harvested together with heat-stressed cells. After being washed with ice-cold PBS, the cells were lysed and separated by SDS-PAGE (10% acrylamide). Western blot analysis was carried out as described in Materials and Methods. Data from one experiment representative of two independent tests are shown. (C) For quantitative analysis of HSP expression, band intensities were determined with NIH Image software. Values were normalized to GAPDH levels. (D) Morphological changes in BDV-infected primary glial cells. Cells were exposed to heat stress at 44°C for 1 h. For morphological analysis, cells were visualized under a phase-contrast microscope. Subpanels: a and b, uninfected; c and d, persistently infected. Stress-treated (b and d) and untreated (a and c) cells were fixed and stained with hematoxylin.

the interrelationship between HSP70 and PKR plays key roles in the regulation of cellular stress responses. Therefore, we finally investigated the expression of PKR in BDV-infected glial cells. We used an antibody specific for autophosphorylated PKR to estimate its active form in these cells. As shown in Fig. 6A, under normal culture conditions, the active form of PKR appeared to be upregulated in persistently infected cells while uninfected cells showed no production of autophosphorylated PKR. Uninfected C6 cells, however, gradually produced the phosphorylated form of PKR with heat treatment, and the protein drastically increased by 6 to 12 h during the recovery period (Fig. 6B). On the other hand, intriguingly, upregulation of PKR expression was not seen in persistently infected C6 cells even under stress (Fig. 6). Although our experiment could not exclude the possibility that the level of autophosphorylated PKR had already reached a peak in the infected cells without a stressor, constant expression of PKR along with no HSP70 induction may provide a possible mechanism by which BDV controls cellular stress responses that could oppose persistence.

DISCUSSION

Our experiments demonstrate that persistent BDV infection may confer instability of HSP70 mRNA in glial cells during the stress response. Although the detailed mechanism by which

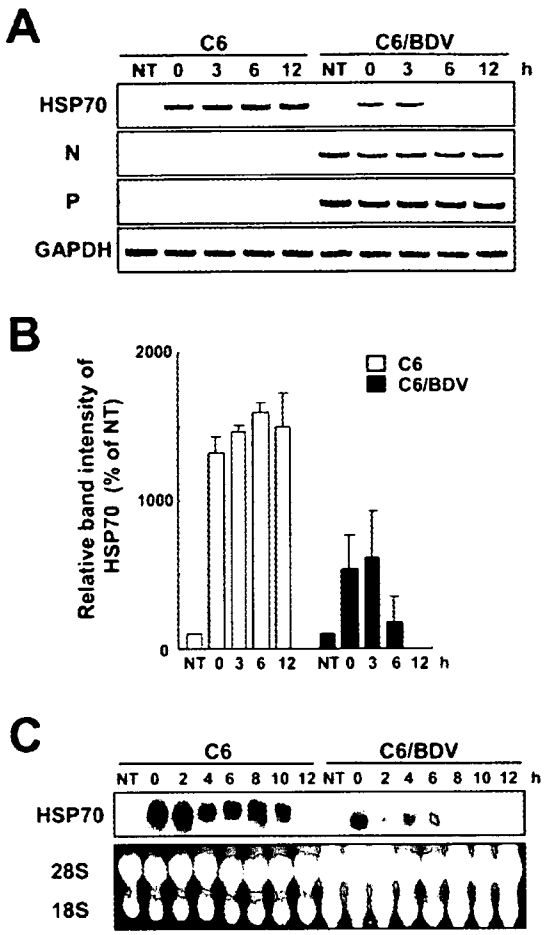

FIG. 5. Stability of HSP70 mRNA in BDV-infected glial cells. C6 cells were exposed to heat stress at 44°C for 1 h and allowed to recover at 37°C for the times indicated. (A) Total RNA was extracted, and semiquantitative RT-PCR for HSP70 mRNA was performed as described in Materials and Methods. As a control for the input RNA, the GAPDH transcript in the cells was also amplified. The amplification products were analyzed by 1.5% agarose gel electrophoresis. Gels were stained with ethidium bromide. The images of agarose gels were captured electronically, and the pixels were inverted. Data from one experiment representative of three independent tests are shown. (B) For quantitative analysis, band intensities were determined with NIH Image software. Values were normalized to GAPDH levels. The data are expressed as the mean plus the standard error. (C) C6 cells were exposed to heat stress at 44°C for 1 h and then allowed to recover at 37°C for various times in the presence of actinomycin D. Total RNA was extracted, and levels of HSP70 mRNA in the extract were analyzed by Northern blotting as described in Materials and Methods. The levels of 28S and 18S rRNAs are also shown. NT, nontreated control cells.

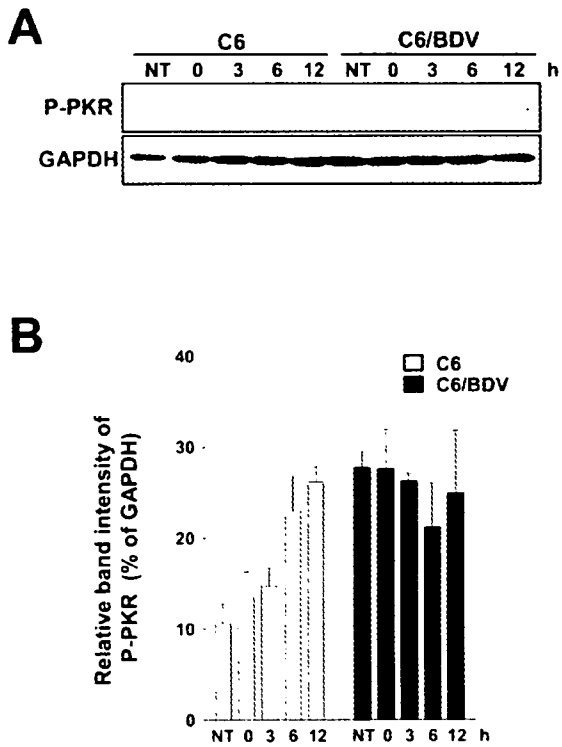

FIG. 6. Induction of autophosphorylated PKR in BDV-infected glial cells during heat stress. (A) After heat shock, uninfected and BDV-infected C6 cells were washed with ice-cold PBS and lysed in lysis buffer. Nontreated control cells (NT) were maintained at 37°C and harvested together with heat-stressed cells. Equivalent amounts of proteins were separated by SDS–PAGE (10% acrylamide). Western blot analysis was carried out to examine relative levels of phosphorylated PKR (P-PKR). Data from one experiment representative of three independent tests are shown. (B) For quantitative analysis, band intensities were determined with NIH Image software. Values were normalized to GAPDH levels. The data are expressed as the mean plus the standard error.

BDV affects the posttranscriptional step of the HSP70 mRNA has remained unclear, the interrelationship between the functions of HSP70 and PKR provides a possibility that aberrant activation of PKR contributes to the instability of the mRNA in BDV-infected cells. PKR is a serine/threonine kinase that is activated by not only RNA or DNA viral infections but also heat stress and several chemical stressors. The best-characterized role of this kinase is the downregulation of mRNA translation via phosphorylation of the α subunit of eukaryotic initiation factor 2, and activation of PKR results in cell growth arrest and apoptosis, as well as increased antiviral interferon activity (5, 52). We propose that PKR function is disrupted in cells persistently infected with BDV, for the following reasons. First, although PKR expression is upregulated in persistently BDV-infected cells in a steady state, the cells did not exhibit any disturbances in proliferation, viability, or BDV protein synthesis (Fig. 1). Second, the constant activation of PKR did not induce HSP70 upregulation in infected cells (Fig. 1 and 2). Third, persistently infected glial cells appeared not to undergo cell death even during the heat shock response period (Fig. 3). In uninfected cells, on the other hand, PKR activation by heat shock seems to be linked to the induction of HSP70 expression and cell death (Fig. 2 and 3). In addition, PKR activation without inhibition of viral protein synthesis was also demonstrated in BDV-infected rat brains (11). Moreover, it has been reported that interferon induction is too weak to eliminate viral activities in BDV-infected mouse brains (47). From these observations, it is likeliest that BDV inhibits PKR function. Recent studies revealed that many viruses can disturb PKR in

infected cells in order to avoid its antiviral actions and cell apoptosis. It is evident that herpes simplex virus infection downregulates eukaryotic initiation factor 2α phosphorylation although PKR is activated (6, 13, 16). Furthermore, simian virus 40 appears to reverse PKR-mediated translational inhibition at a step downstream of PKR activation (13, 39). Thus, one might argue that persistent BDV infection also inhibits the PKR signaling pathway somewhere downstream of PKR autophosphorylation. Note that we found some discrepancy between the expression kinetics of HSP70 protein and mRNA in BDV-infected cells (Fig. 2 and 5). We found weak activation of HSP70 protein in persistently infected C6 cells at 6 and 12 h after heat stress, whereas HSP70 mRNA was detected at 0 and 3 h by RT-PCR. Interestingly, a previous study has also demonstrated that slight activation of HSP70 is detected later than expression of its mRNA for 4 h in a PKR-negative cell line (55). On the basis of these observations, it is possible that inhibition of the PKR pathway may also affect the delayed accumulation of HSP70 in stress-treated cells.

Inhibition of HSP70 induction might be critical for the survival of the virus in host cells. HSP70 is known to play direct roles in interfering with viral protein synthesis and replication (8, 35, 42). In addition, this protein can facilitate viral antigen presentation in cells such as macrophages and dendrites (46, 49). Furthermore, elevations of intracellular HSP levels have been shown to improve cell tolerance to inflammatory cytokines, such as tumor necrosis factor alpha and interleukin-1 (1). Moreover, the HSP70 present on the cell surface functions as a recognition molecule for natural killer cells (28). These observations demonstrated that HSP70 plays important roles in viral elimination in infected host cells. Thus, suppression of HSP70 expression could be an effective strategy used by BDV to maintain long-lasting persistence.

In the CNS, a number of HSPs are constitutively or inducibly expressed, and their upregulation and presence are connected to the neuroprotection of neuronal and glial cells (40, 53). It is generally accepted that HSP70 is highly upregulated by hyperthermia and a variety of other stressors in astrocytes, oligodendrocytes, and microglia, and the released HSP70 can enhance neuronal stress tolerance (40, 53). Another study has also demonstrated that HSP70 causes microglial activation and an increase in cytokine production, which might contribute to neuroprotective roles in infected brains (18). Furthermore, large HSPs are known to interact with the cytoskeleton and assist in the proper assembly and spatial organization of cells (20). In neuronal cells, cytoskeletal stability could be absolutely necessary for synaptic plasticity and CNS development. Indeed, it has been reported that HSP70 localizes to the synapses after stress induction and also that the expression of HSP70 protects synapse formation, as well as synaptic transmission (2, 31, 40). Interestingly, we also found that a human neuroblastoma cell line, SK-N-SH, shows delayed expression of HSP70 during persistent BDV infection. Expression of HSP70 was detected only from 12 h after heat shock in infected SK-N-SH cells, while uninfected control cells rapidly induced HSP70 from 3 h after heat treatment (data not shown). These observations suggest that inhibition of HSP70 expression during BDV infection may have deleterious effects on synaptic plasticity, especially under stress. Moreover, HSP70 has been revealed to be constitutively expressed in the rat CNS from postnatal development to maturity (4), suggesting that inhibition of HSP70 expression in developing brains may cause developmental damage of the CNS, as is shown in the brains of rat neonatally infected with BDV. Further study is needed to understand the effects of HSP70 inhibition in the brains of animals persistently infected with BDV.

ACKNOWLEDGMENTS

M.Y. is supported by the special research fellow program of the Japan Society for the Promotion of Science (JSPS). This study was supported by grants from the Ministry of Education, Culture, Sports, Science and Technology of Japan, a grant-in-aid from the Zoonosis Control Project of the Ministry of Agriculture, Forestry and Fisheries of Japan, and a Research Grant for Nervous and Mental Disorders from the Ministry of Health, Labor and Welfare of Japan.

REFERENCES

1. **Asea, A., S. K. Kraeft, E. A. Kurt-Jones, M. A. Stevenson, L. B. Chen, R. W. Finberg, G. C. Koo, and S. K. Calderwood.** 2000. HSP70 stimulates cytokine production through a CD14-dependent pathway, demonstrating its dual role as a chaperone and cytokine. Nat. Med. **6**:435–442.
2. **Bechtold, D. A., S. J. Rush, and I. R. Brown.** 2000. Localization of the heat-shock protein Hsp70 to the synapse following hyperthermic stress in the brain. J. Neurochem. **74**:641–646.
3. **Beck, J., and M. Nassal.** 2003. Efficient Hsp90-independent in vitro activation by Hsc70 and Hsp40 of duck hepatitis B virus reverse transcriptase, an assumed Hsp90 client protein. J. Biol. Chem. **278**:36128–36138.
4. **Bodega, G., C. Hernandez, I. Suarez, M. Martin, and B. Fernandez.** 2002. HSP70 constitutive expression in rat central nervous system from postnatal development to maturity. J. Histochem. Cytochem. **50**:1161–1168.
5. **Chawla-Sarkar, M., D. J. Lindner, Y. F. Liu, B. R. Williams, G. C. Sen, R. H. Silverman, and E. C. Borden.** 2003. Apoptosis and interferons: role of interferon-stimulated genes as mediators of apoptosis. Apoptosis **8**:237–249.
6. **Cheng, G., K. Yang, and B. He.** 2003. Dephosphorylation of eIF-2α mediated by the $\gamma_1$34.5 protein of herpes simplex virus type 1 is required for viral response to interferon but is not sufficient for efficient viral replication. J. Virol. **77**:10154–10161.
7. **Chromy, L. R., J. M. Pipas, and R. L. Garcea.** 2003. Chaperone-mediated in vitro assembly of polyomavirus capsids. Proc. Natl. Acad. Sci. USA **100**: 10477–10482.
8. **Conti, C., A. De Marco, P. Mastromarino, P. Tomao, and M. G. Santoro.** 1999. Antiviral effect of hyperthermic treatment in rhinovirus infection. Antimicrob. Agents Chemother. **43**:822–829.
9. **Cubitt, B., C. Oldstone, and J. C. de la Torre.** 1994. Sequence and genome organization of Borna disease virus. J. Virol. **68**:1382–1396.
10. **de la Torre, J. C.** 2002. Molecular biology of Borna disease virus and persistence. Front. Biosci. **7**:D569–D579.
11. **Dietzschold, B., K. Morimoto, and D. C. Hooper.** 2001. Mechanisms of virus-induced neuronal damage and the clearance of viruses from the CNS. Curr. Top. Microbiol. Immunol. **253**:145–155.
12. **Eisenman, L. M., R. Brothers, M. H. Tran, R. B. Kean, G. M. Dickson, B. Dietzschold, and D. C. Hooper.** 1999. Neonatal Borna disease virus infection in the rat causes a loss of Purkinje cells in the cerebellum. J. Neurovirol. **5**:181–189.
13. **Gale, M., Jr., and M. G. Katze.** 1998. Molecular mechanisms of interferon resistance mediated by viral-directed inhibition of PKR, the interferon-induced protein kinase. Pharmacol. Ther. **78**:29–46.
14. **Guerrero, C. A., D. Bouyssounade, S. Zarate, P. Isa, T. Lopez, R. Espinosa, P. Romero, E. Mendez, S. Lopez, and C. F. Arias.** 2002. Heat shock cognate protein 70 is involved in rotavirus cell entry. J. Virol. **76**:4096–4102.
15. **Hans, A., S. Syan, C. Crosio, P. Sassone-Corsi, M. Brahic, and D. Gonzalez-Dunia.** 2001. Borna disease virus persistent infection activates mitogen-activated protein kinase and blocks neuronal differentiation of PC12 cells. J. Biol. Chem. **276**:7258–7265.
16. **He, B., J. Chou, R. Brandimarti, I. Mohr, Y. Gluzman, and B. Roizman.** 1997. Suppression of the phenotype of $\gamma_1$34.5$^-$ herpes simplex virus 1: failure of activated RNA-dependent protein kinase to shut off protein synthesis is associated with a deletion in the domain of the α47 gene. J. Virol. **71**:6049–6054.
17. **Hornig, M., M. Solbrig, N. Horscroft, H. Weissenbock, and W. I. Lipkin.** 2001. Borna disease virus infection of adult and neonatal rats: models for neuropsychiatric disease. Curr. Top. Microbiol. Immunol. **253**:157–177.
18. **Kakimura, J., Y. Kitamura, K. Takata, M. Umeki, S. Suzuki, K. Shibagaki, T. Taniguchi, Y. Nomura, P. J. Gebicke-Haerter, M. A. Smith, G. Perry, and S. Shimohama.** 2002. Microglial activation and amyloid-beta clearance induced by exogenous heat-shock proteins. FASEB J. **16**:601–603.
19. **Kamitani, W., Y. Shoya, T. Kobayashi, M. Watanabe, B. J. Lee, G. Zhang, K.**

Tomonaga, and K. Ikuta. 2001. Borna disease virus phosphoprotein binds a neurite outgrowth factor, amphoterin/HMG-1. J. Virol. **75**:8742–8751.
20. **Liang, P., and T. H. MacRae.** 1997. Molecular chaperones and the cytoskeleton. J. Cell Sci. **110**:1431–1440.
21. **Lindquist, S., and E. A. Craig.** 1988. The heat-shock proteins. Annu. Rev. Genet. **22**:631–677.
22. **Ludwig, H., and L. Bode.** 2000. Borna disease virus: new aspects on infection, disease, diagnosis and epidemiology. Rev. Sci. Tech. **19**:259–288.
23. **Mao, H., F. Li, K. Ruchalski, D. D. Mosser, J. H. Schwartz, Y. Wang, and S. C. Borkan.** 2003. hsp72 inhibits focal adhesion kinase degradation in ATP-depleted renal epithelial cells. J. Biol. Chem. **278**:18214–18220.
24. **Mathew, A., and R. I. Morimoto.** 1998. Role of the heat-shock response in the life and death of proteins. Ann. N. Y. Acad. Sci. **851**:99–111.
25. **Melville, M. W., S. L. Tan, M. Wambach, J. Song, R. I. Morimoto, and M. G. Katze.** 1999. The cellular inhibitor of the PKR protein kinase, $P58^{IPK}$, is an influenza virus-activated co-chaperone that modulates heat shock protein 70 activity. J. Biol. Chem. **274**:3797–3803.
26. **Momose, F., T. Naito, K. Yano, S. Sugimoto, Y. Morikawa, and K. Nagata.** 2002. Identification of Hsp90 as a stimulatory host factor involved in influenza virus RNA synthesis. J. Biol. Chem. **277**:45306–45314.
27. **Morimoto, R. I.** 1993. Cells in stress: transcriptional activation of heat shock genes. Science **259**:1409–1410.
28. **Multhoff, G.** 2002. Activation of natural killer cells by heat shock protein 70. Int. J. Hyperthermia **18**:576–585.
29. **Nakamura, Y., H. Takahashi, Y. Shoya, T. Nakaya, M. Watanabe, K. Tomonaga, K. Iwahashi, K. Ameno, N. Momiyama, H. Taniyama, T. Sata, T. Kurata, J. C. de la Torre, and K. Ikuta.** 2000. Isolation of Borna disease virus from human brain tissue. J. Virol. **74**:4601–4611.
30. **Oglesbee, M. J., M. Pratt, and T. Carsillo.** 2002. Role for heat shock proteins in the immune response to measles virus infection. Viral Immunol. **15**:399–416.
31. **Ohtsuka, K., and T. Suzuki.** 2000. Roles of molecular chaperones in the nervous system. Brain Res. Bull. **53**:141–146.
32. **Palazzo, A. F., C. H. Eng, D. D. Schlaepfer, E. E. Marcantonio, and G. G. Gundersen.** 2004. Localized stabilization of microtubules by integrin- and FAK-facilitated Rho signaling. Science **303**:836–839.
33. **Pang, Q., T. A. Christianson, W. Keeble, T. Koretsky, and G. C. Bagby.** 2002. The anti-apoptotic function of Hsp70 in the interferon-inducible double-stranded RNA-dependent protein kinase-mediated death signaling pathway requires the Fanconi anemia protein, FANCC. J. Biol. Chem. **277**:49638–49643.
34. **Pang, Q., W. Keeble, T. A. Christianson, G. R. Faulkner, and G. C. Bagby.** 2001. FANCC interacts with Hsp70 to protect hematopoietic cells from IFN-γ/TNF-α-mediated cytotoxicity. EMBO J. **20**:4478–4489.
35. **Pica, F., A. T. Palamara, A. Rossi, A. De Marco, C. Amici, and M. G. Santoro.** 2000. Δ^{12}-prostaglandin J_2 is a potent inhibitor of influenza A virus replication. Antimicrob. Agents Chemother. **44**:200–204.
36. **Planz, O., S. Pleschka, K. Oesterle, F. Berberich-Siebelt, C. Ehrhardt, L. Stitz, and S. Ludwig.** 2003. Borna disease virus nucleoprotein interacts with the CDC2-cyclin B1 complex. J. Virol. **77**:11186–11192.
37. **Pletnikov, M. V., D. Gonzalez-Dunia, and L. Stitz.** 2002. Experimental infection: pathogenesis of neurobehavioral disease, p. 125–178. *In* K. M. Carbone (ed.), Borna disease virus and its role in neurobehavioral disease. ASM Press, Washington, D.C.
38. **Pletnikov, M. V., T. H. Moran, and K. M. Carbone.** 2002. Borna disease virus infection of the neonatal rat: developmental brain injury model of autism spectrum disorders. Front. Biosci. **7**:D593–D607.
39. **Rajan, P., S. Swaminathan, J. Zhu, C. N. Cole, G. Barber, M. J. Tevethia, and B. Thimmapaya.** 1995. A novel translational regulation function for the simian virus 40 large-T antigen gene. J. Virol. **69**:785–795.
40. **Richter-Landsberg, C., and O. Goldbaum.** 2003. Stress proteins in neural cells: functional roles in health and disease. Cell. Mol. Life Sci. **60**:337–349.
41. **Rott, R., and H. Becht.** 1995. Natural and experimental Borna disease in animals. Curr. Top. Microbiol. Immunol. **190**:17–30.
42. **Rozera, C., A. Carattoli, A. De Marco, C. Amici, C. Giorgi, and M. G. Santoro.** 1996. Inhibition of HIV-1 replication by cyclopentenone prostaglandins in acutely infected human cells. Evidence for a transcriptional block. J. Clin. Investig. **97**:1795–1803.
43. **Rubin, S. A., P. Sylves, M. Vogel, M. Pletnikov, T. H. Moran, G. J. Schwartz, and K. M. Carbone.** 1999. Borna disease virus-induced hippocampal dentate gyrus damage is associated with spatial learning and memory deficits. Brain Res. Bull. **48**:23–30.
44. **Santoro, M. G.** 1996. Viral infection. EXS **77**:337–357.
45. **Sharp, F. R., S. M. Massa, and R. A. Swanson.** 1999. Heat-shock protein protection. Trends Neurosci. **22**:97–99.
46. **Srivastava, P.** 2002. Roles of heat-shock proteins in innate and adaptive immunity. Nat. Rev. Immunol. **2**:185–194.
47. **Staeheli, P., M. Sentandreu, A. Pagenstecher, and J. Hausmann.** 2001. Alpha/beta interferon promotes transcription and inhibits replication of Borna disease virus in persistently infected cells. J. Virol. **75**:8216–8223.
48. **Stitz, L., T. Bilzer, and O. Planz.** 2002. The immunopathogenesis of Borna disease virus infection. Front. Biosci. **7**:D541–D555.
49. **Todryk, S., A. A. Melcher, N. Hardwick, E. Linardakis, A. Bateman, M. P. Colombo, A. Stoppacciaro, and R. G. Vile.** 1999. Heat shock protein 70 induced during tumor cell killing induces Th1 cytokines and targets immature dendritic cell precursors to enhance antigen uptake. J. Immunol. **163**:1398–1408.
50. **Tomonaga, K.** 2004. Virus-induced neurobehavioral disorders: mechanisms and implications. Trends Mol. Med. **10**:71–77.
51. **Tomonaga, K., T. Kobayashi, and K. Ikuta.** 2002. Molecular and cellular biology of Borna disease virus infection. Microbes Infect. **4**:491–500.
52. **Williams, B. R.** 1999. PKR: a sentinel kinase for cellular stress. Oncogene **18**:6112–6120.
53. **Yenari, M. A.** 2002. Heat shock proteins and neuroprotection. Adv. Exp. Med. Biol. **513**:281–299.
54. **Zhang, G., T. Kobayashi, W. Kamitani, S. Komoto, M. Yamashita, S. Baba, H. Yanai, K. Ikuta, and K. Tomonaga.** 2003. Borna disease virus phosphoprotein represses p53-mediated transcriptional activity by interference with HMGB1. J. Virol. **77**:12243–12251.
55. **Zhao, M., D. Tang, S. Lechpammer, A. Hoffman, A. Asea, M. A. Stevenson, and S. K. Calderwood.** 2002. Double-stranded RNA-dependent protein kinase (*pkr*) is essential for thermotolerance, accumulation of HSP70, and stabilization of ARE-containing HSP70 mRNA during stress. J. Biol. Chem. **277**:44539–44547.

JOURNAL OF CLINICAL MICROBIOLOGY, May 2005, p. 2474–2476 Vol. 43, No. 5
0095-1137/05/$08.00+0 doi:10.1128/JCM.43.5.2474–2476.2005

Comparative Molecular Analysis of *Haemophilus influenzae* Isolates from Young Children with Acute Lower Respiratory Tract Infections and Meningitis in Hanoi, Vietnam

Hiroshi Watanabe,[1]* Chiharu Kaji,[1] Dang Duc Anh,[2] Phan Le Thanh Huong,[2] Nguyen Thi Hien Anh,[2] Vu Thi Huong,[2] Hoang Vu Mai Phuong,[2] Ngo Thi Thi,[3] Pham Thi Suu,[3] Nguyen Thi Thu Nguyet,[3] Olivia Sebastian Rusizoka,[1] Kiwao Watanabe,[1] Tsuyoshi Nagatake,[1] and Kazunori Oishi[1]

Department of Internal Medicine, Institute of Tropical Medicine, Nagasaki University, Nagasaki, Japan,[1] and National Institute of Hygiene and Epidemiology[2] and National Institute of Pediatrics,[3] Hanoi, Vietnam

Received 10 December 2004/Accepted 11 December 2004

Thirty-seven *Haemophilus influenzae* strains from nasopharyngeal swabs (NP) and 44 *H. influenzae* strains from cerebrospinal fluid (CSF) were investigated. Of the 37 *H. influenzae* isolates from NP, the serotypes of 30 isolates were nontypeable, 4 were type b, 2 were type c, and 1 was type a, whereas all of the 44 isolates from CSF were type b. The MICs of 16 antibiotics for the *H. influenzae* isolates from NP and CSF were similar, and no β-lactamase-negative ampicillin-resistant strain was found. Molecular typing by pulsed-field gel electrophoresis (PFGE) showed that the 37 *H. influenzae* strains from NP had 22 PFGE patterns, with none predominating, and the 44 *H. influenzae* strains from CSF had 9 PFGE patterns, with patterns α (22 isolates) and β (12 isolates) predominating. Our results indicate that two predominant types of *H. influenzae* type b strains have the potential to spread among children with meningitis in Hanoi, Vietnam.

Nontypeable *Haemophilus influenzae* (NTHi) can cause a variety of infections, including otitis media, bronchitis, and pneumonia (7), whereas *H. influenzae* type b (Hib) is a common cause of meningitis in children (11). Hib infection rates have been dramatically reduced in countries that have implemented Hib conjugate vaccine programs as part of routine infant immunizations (10). It has also recently been reported that β-lactamase-negative ampicillin (AMP)-resistant (BLNAR) strains have increased in some countries (6, 12), although their global prevalence remains low (4, 5). The aim of our study was to investigate the characteristics of *H. influenzae* among children less than 5 years of age in Vietnam.

Thirty-seven *H. influenzae* strains were isolated from the nasopharyngeal swabs (NP) of 37 children aged 2 to 60 months (mean age, 11 months) who were diagnosed with acute lower respiratory tract infections between 2001 and 2002, and 44 *H. influenzae* strains were isolated from the cerebrospinal fluid (CSF) of 44 children aged 1 to 24 months (mean age, 9 months) who were diagnosed with meningitis between 2002 and 2003, in Hanoi, Vietnam. No patient with an acute lower respiratory tract infection overlapped a patient with meningitis. *H. influenzae* isolates were serotyped by slide agglutination with antisera purchased from Difco Laboratories (Detroit, Mich.), and β-lactamase production was detected by a disk impregnated with nitrocefin (Becton Dickinson, Sparks, Md.). PCR was carried out for *H. influenzae* isolates by using mixed primers (Wakunaga Pharmaceutical Co., Hiroshima, Japan), as described previously (3). MICs were determined by the agar dilution method according to the NCCLS guidelines (8). The susceptibilities of 81 *H. influenzae* isolates to the following 16 antibiotics were tested: penicillin G (Meiji Seika Kaisha, Tokyo, Japan), AMP (Meiji Seika Kaisha), amoxicillin-clavulanic acid (AMC) (GlaxoSmithKline K.K., Tokyo, Japan), cefatrizine (Taiyo Yakuhin Co., Nagoya, Japan), cefuroxime (Sankyo Co., Tokyo, Japan), ceftriaxone (Chugai Pharmaceutical Co., Tokyo, Japan), cefotaxime (Aventis Pharma, Tokyo, Japan), imipenem (Banyu Pharmaceutical Co., Tokyo, Japan), minocycline [Lederle (Japan), Tokyo, Japan], chloramphenicol (Sankyo Co.), clarithromycin (Taisho Pharmaceutical Co., Tokyo, Japan), erythromycin (Dainippon Pharmaceutical Co., Osaka, Japan), gentamicin (Schering-Plough K.K., Osaka, Japan), levofloxacin (Daiichi Pharmaceutical Co., Tokyo, Japan), norfloxacin (Kyorin Pharmaceutical Co., Tokyo, Japan), and sulfamethoxazole-trimethoprim (Shionogi & Co., Osaka, Japan). After digestion with SmaI (Takara Shuzo Co., Shiga, Japan), pulsed-field gel electrophoresis (PFGE) was performed on the 37 *H. influenzae* isolates from the NP and the 44 *H. influenzae* isolates from the CSF, as described previously (16), and the interpretation of PFGE patterns was based on the criteria described by Tenover et al. (13).

Of the 37 *H. influenzae* isolates from NP, the serotypes of 30 isolates were nontypeable, 4 were type b, 2 were type c, and 1 was type a, whereas the 44 isolates from CSF were all type b. Twenty-six strains (70.3%) from NP and 23 strains (52.3%) from CSF were β-lactamase producing, and the remaining strains were β-lactamase negative by the nitrocefin disk assay. PCR analysis to identify the resistance genes indicated that 25 strains from NP and 21 strains from CSF were β-lactamase-producing AMP-resistant isolates which had the TEM-1-type β-lactamase gene; 11 strains from NP and 22 strains from CSF were β-lactamase-negative AMP-susceptible isolates, all of which lacked all resistance genes; and 1 strain each from NP and CSF were β-lactamase-producing AMC-resistant isolates

* Corresponding author. Mailing address: Department of Internal Medicine, Institute of Tropical Medicine, Nagasaki University, 1-12-4 Sakamoto, Nagasaki 852-8523, Japan. Phone: 81 (95) 849-7842. Fax: 81 (95) 849-7843. E-mail: h-wata@net.nagasaki-u.ac.jp.

TABLE 1. Distribution of MICs against 16 antibiotics for *H. influenzae* strains isolated from nasopharyngeal swabs and cerebrospinal fluid from children in Vietnam

Antibiotic	MIC (μg/ml) for isolates from:					
	NP (n = 37)			CSF (n = 44)		
	Range	50%	90%	Range	50%	90%
Penicillin G	0.5–128	16	32	≤0.004–128	2	32
Ampicillin	0.25–64	8	32	0.125–32	1	8
Amoxicillin-clavulanic acid	0.25–2	0.5	0.5	0.25–1	0.25	0.25
Cefatrizine	2–32	4	8	2–16	4	16
Cefuroxime	0.5–4	1	4	0.016–4	1	2
Ceftriaxone	≤0.004–0.032	0.008	0.016	≤0.004–0.032	0.008	0.008
Cefotaxime	0.008–0.125	0.032	0.032	≤0.004–0.125	0.032	0.063
Imipenem	0.25–4	2	2	0.25–1	0.25	1
Minocycline	0.5–2	1	2	0.5–2	1	1
Chloramphenicol	0.5–16	4	8	0.5–16	8	16
Clarithromycin	0.25–16	8	16	4–16	8	8
Erythromycin	0.25–4	4	4	0.016–8	2	4
Gentamicin	1–2	1	2	0.016–2	0.5	2
Levofloxacin	0.016–0.063	0.032	0.032	≤0.004–0.032	0.032	0.032
Norfloxacin	0.063–0.125	0.125	0.125	0.063–0.125	0.063	0.125
Sulfamethoxazole-trimethoprim	1–≥128	≥128	≥128	0.032–≥128	128	≥128

which had the TEM-1-type β-lactamase gene and the *ftsI* gene with the same substitution as the low-BLNAR strains. Although all isolates from NP which had the TEM-1-type β-lactamase gene were β-lactamase producing by the nitrocefin disk assay, one isolate from CSF which had the TEM-1-type β-lactamase gene was β-lactamase negative and two isolates from CSF which did not have the TEM-1-type β-lactamase gene were β-lactamase producing by the nitrocefin disk assay. No BLNAR strain was found. Table 1 shows the MIC range, the MICs at which 50% of isolates were inhibited (MIC_{50}), and the MIC_{90} of 16 antibiotics for 37 *H. influenzae* isolates from NP and 44 *H. influenzae* isolates from CSF. Although the MICs of the *H. influenzae* isolates from NP against penicillin G and AMP appear to be higher than those from CSF, the antimicrobial susceptibilities of the *H. influenzae* isolates from NP and CSF were similar. Molecular typing by pulsed-field gel electrphoresis (PFGE) showed that the 37 *H. influenzae* strains from NP had 22 PFGE patterns (A to V), without any predominant pattern (Fig. 1). The PFGE patterns of *H. influenzae* types a, b, and c were different from those of NTHi. Four isolates of type b had two PFGE patterns (I and K), and two isolates of type c had two PFGE patterns (H and Q). Forty-four *H. influenzae* strains from CSF had nine PFGE patterns (α to ι), with patterns α (22 isolates) and β (12 isolates) predominating. The PFGE patterns of 4 *H. influenzae* type b strains from NP were quite different from those of the 44 *H. influenzae* type b strains from CSF (Fig. 2).

Infants and young children tend to acquire *H. influenzae* in the upper respiratory tract because of their low immunity (16), and subsequent colonization can become a risk factor for invasive diseases caused by *H. influenzae* (2, 11). Since it has recently been reported that BLNAR NTHi and Hib have increased in some countries (3, 6, 12), the primary objective of this study was to investigate such resistant strains among children in Vietnam. In fact, no BLNAR strains were found in either NP or CSF, although more than half the isolates were β-lactamase producing and had the TEM-1-type β-lactamase gene. Hib remains the major cause of meningitis after the introduction of Hib vaccine in many advanced nations, because that vaccine is not usually available in Vietnam (14). Therefore, a secondary objective of this study was to examine the transmission route of *H. influenzae*. It has recently been reported that children can acquire *H. influenzae* at day care centers (9, 16) or from their parents at home (15). Our PFGE studies showed that NTHi did not have dominant genetic patterns but that Hib had two dominant genetic patterns. The results provide evidence to show that at least two types of Hib strains are spreading horizontally among children with meningitis in Vietnam. The Hib conjugate vaccine appears to be effective, not only for the prevention of invasive diseases, but also for the reduction of nasopharyngeal carriage in young children (1, 10).

In conclusion, our results demonstrate that BLNAR strains are not prevalent and that two predominant types of Hib

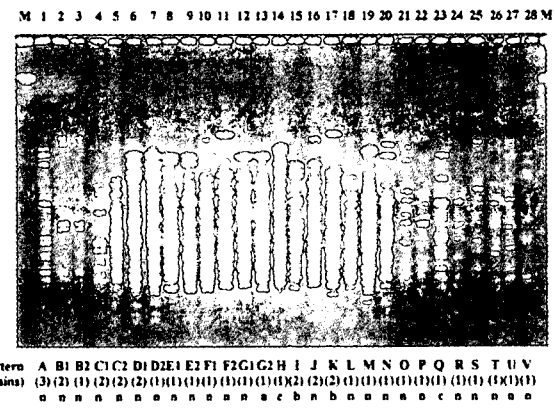

FIG. 1. PFGE patterns of SmaI-digested DNA from 37 *H. influenzae* isolates from NP of 37 children with acute lower respiratory tract infections. Molecular typing by PFGE demonstrated that 37 *H. influenzae* strains from the NP had 22 PFGE patterns (A to V), without any predominant pattern. The PFGE patterns of *H. influenzae* types a, b, and c were different from those of the nontypeable strains.

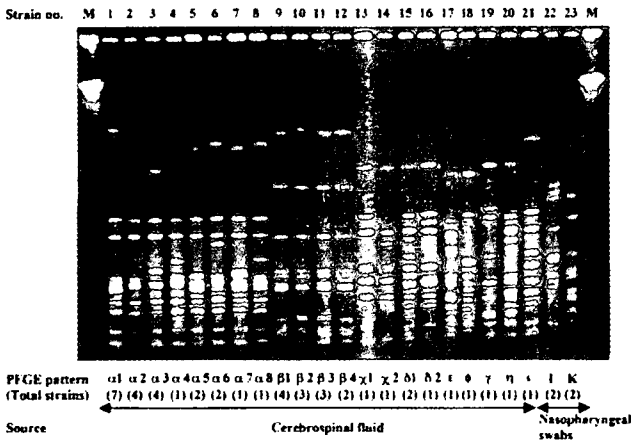

FIG. 2. PFGE patterns of SmaI-digested DNA from 48 Hib isolates from the CSF of 44 children with meningitis and the NP of 4 children with acute lower respiratory tract infections. Molecular typing by PFGE demonstrated that the 44 Hib strains from the CSF had nine PFGE patterns (α to ι), with patterns α (22 isolates) and β (12 isolates) predominating. PFGE patterns of 4 Hib strains from the NP were quite different from those of 44 Hib strains from CSF.

strains have the potential for spreading among children with meningitis in Hanoi, Vietnam. Therefore, the introduction of the Hib conjugate vaccine for young children should be considered in order to prevent invasive diseases caused by Hib.

We thank Akihiro Wada (Department of Bacteriology, Institute of Tropical Medicine, Nagasaki University), Chieko Shimauchi (Miyazaki Prefectural Nursing University), and Matsuhisa Inoue (Kitasato University School of Medicine) for help with completion of the PFGE studies. We also thank Yoko Takashima and Naoko Kitajima (Department of Internal Medicine, Institute of Tropical Medicine, Nagasaki University) for help with PCR studies.

This study was supported by the Core University Program, sponsored by the Japan Society for the Promotion of Science (JSPS).

REFERENCES

1. **Barbour, M. L., R. T. Mayon-White, C. Coles, D. W. Crook, and E. R. Moxon.** 1995. The impact of conjugate vaccine on carriage of *Haemophilus influenzae* type b. J. Infect. Dis. **171**:93–98.
2. **Faden, H., L. Duffy, R. Wasielewski, J. Wolf, D. Krystofik, and Y. Tung.** 1997. Relationship between nasopharyngeal colonization and the development of otitis media in children. J. Infect. Dis. **175**:1440–1445.
3. **Hasegawa, K., N. Chiba, R. Kobayashi, S. Y. Murayama, S. Iwata, K. Sunakawa, and K. Ubukata.** 2004. Rapidly increasing prevalence of β-lactamase-nonproducing, ampicillin-resistant *Haemophilus influenzae* type b in patients with meningitis. Antimicrob. Agents Chemother. **48**:1509–1514.
4. **Hoban, D., and D. Felmingham.** 2002. The PROTEKT surveillance study: antimicrobial susceptibility of *Haemophilus influenzae* and *Moraxella catarrhalis* from community-acquired respiratory tract infections. J. Antimicrob. Chemother. **50**:49–59.
5. **Karlowsky, J. A., I. A. Critchley, R. S. Blosser-Middleton, E. A. Karginova, M. E. Jones, C. Thornsberry, and D. F. Sahm.** 2002. Antimicrobial surveillance of *Haemophilus influenzae* in the United States during 2000–2001 leads to detection of clonal dissemination of a beta-lactamase-negative and ampicillin-resistant strain. J. Clin. Microbiol. **40**:1063–1066.
6. **Marco, F., J. Garcia-de-Lomas, C. Garcia-Rey, E. Bouza, L. Aguilar, C. Fernandez-Mazarrasa, and the Spanish Surveillance Group for Respiratory Pathogens.** 2001. Antimicrobial susceptibilities of 1,730 *Haemophilus influenzae* respiratory tract isolates in Spain in 1998–1999. Antimicrob. Agents Chemother. **45**:3226–3228.
7. **Murphy, T. F., and M. A. Apicella.** 1987. Nontypeable *Haemophilus influenzae*: a review of clinical aspects, surface antigens, and the human immune response to infection. Rev. Infect. Dis. **9**:1–15.
8. **National Committee for Clinical Laboratory Standards.** 1998. Methods for dilution antimicrobial susceptibility tests for bacteria that grow aerobically. Approved standard M7-A4. National Committee for Clinical Laboratory Standards, Wayne, Pa.
9. **Peerbooms, P. G., M. N. Engelen, D. A. Stokman, B. H. van Benthem, M. L. van Weert, S. M. Bruisten, A. van Belkum, and R. A. Coutinho.** 2002. Nasopharyngeal carriage of potential bacterial pathogens related to day care attendance, with special reference to the molecular epidemiology of *Haemophilus influenzae*. J. Clin. Microbiol. **40**:2832–2836.
10. **Peltola, H.** 2000. Worldwide *Haemophilus influenzae* type b disease at the beginning of the 21st century: global analysis of the disease burden 25 years after the use of the polysaccharide vaccine and a decade after the advent of conjugates. Clin. Microbiol. Rev. **13**:302–317.
11. **Saito, M., K. Okada, K. Takemori, and S. Yoshida.** 2000. Clonal spread of an invasive strain of *Haemophilus influenzae* type b among nursery contacts accompanied by a high carriage rate of non-disease-associated strains. J. Med. Microbiol. **49**:845–847.
12. **Suzuki, K., T. Nishimura, and S. Baba.** 2003. Current status of bacterial resistance in the otolaryngology field: results from the Second Nationwide Survey in Japan. J. Infect. Chemother. **9**:46–52.
13. **Tenover, F. C., R. D. Arbeit, R. V. Goering, P. A. Mickelsen, B. E. Murray, D. H. Persing, and B. Swaminathan.** 1995. Interpreting chromosomal DNA restriction patterns produced by pulsed-field gel electrophoresis: criteria for bacterial strain typing. J. Clin. Microbiol. **33**:2233–2239.
14. **Tran, T. T., Q. T. Le, T. N. Tran, N. T. Nguyen, F. K. Pedersen, and M. Schlumberger.** 1998. The etiology of bacterial pneumonia and meningitis in Vietnam. Pediatr. Infect. Dis. J. **17**(Suppl. 9):S192–S194.
15. **Watanabe, H., K. Hoshino, R. Sugita, N. Asoh, K. Watanabe, K. Oishi, and T. Nagatake.** 2004. Possible high rate of transmission of nontypeable *Haemophilus influenzae* including β-lactamase-negative ampicillin-resistant strains between children and their parents. J. Clin. Microbiol. **42**:362–365.
16. **Yano, H., M. Suetake, A. Kuga, K. Irinoda, R. Okamoto, T. Kobayashi, and M. Inoue.** 2000. Pulsed-field gel electrophoresis analysis of nasopharyngeal flora in children attending a day care center. J. Clin. Microbiol. **38**:625–629.

MAJOR ARTICLE

Quantitative Analysis of Kaposi Sarcoma–Associated Herpesvirus (KSHV) in KSHV-Associated Diseases

Yasuko Asahi-Ozaki, Yuko Sato, Takayuki Kanno, Tetsutaro Sata, and Harutaka Katano

Department of Pathology, National Institute of Infectious Diseases, Shinjuku, Tokyo, Japan

Background. Accurate numbers of copies of Kaposi sarcoma–associated herpesvirus (KSHV) and numbers of virus-infected cells in lesions caused by KSHV-associated diseases are unknown.

Methods. Quantitative polymerase chain reaction (PCR) and computerized imaging of immunohistochemical analysis were performed on pathologic sections of samples from persons with KSHV-associated diseases.

Results. Real-time PCR and semiquantitative PCR–Southern blotting demonstrated that DNA extracted from biopsy samples of KS lesions contained ~1–2 viral copies/cell. KSHV-associated lymphoma contained 10–50 viral copies/cell. Computerized-image analysis demonstrated that ~49% of cells expressed KSHV-encoded latency-associated nuclear antigen in KS biopsy samples. On the basis of results of real-time PCR and computerized-image analysis, the predicted number of viral copies was 3.2 viral copies/cell in KS lesions. Computerized-image analysis also revealed that the expression of open-reading frame (ORF)–50 protein, an immediate early protein of KSHV, was very rare in KS lesions, which implies that they were mainly composed of proliferating cells latently infected with KSHV. In multicentric Castleman disease lesions, 25% of virus-infected cells expressed ORF50 protein, which suggests the frequent lytic replication of KSHV.

Conclusions. Numbers of viral copies and of virus-positive cells vary among KSHV-associated diseases, which suggests different mechanisms of viral pathogenesis. The combination of real-time PCR and computerized-image analysis provides a useful tool for the assessment of the number of viral copies in KSHV-associated diseases.

Kaposi sarcoma–associated herpesvirus (KSHV, also called human herpesvirus [HHV]–8) has been detected by polymerase chain reaction (PCR) and immunohistochemical analysis in almost all cases of KS, regardless of HIV infection status [1–6]. Primary effusion lymphoma (PEL) is also a KSHV-associated disease [7], and KSHV-associated solid lymphoma has been reported to be a variant of PEL that forms solid tumors [8, 9]. Some, but not all, cases of multicentric Castleman disease (MCD) are also KSHV positive [10, 11].

Similarly to other herpesviruses, KSHV has 2 phases of infection: lytic and latent [1, 12]. During the lytic phase, KSHV replicates in infected cells, which results in cell lysis. However, the virus does not replicate in latently infected cells, although they harbor viral episomes and express several KSHV-encoded latency-associated proteins, such as latency-associated nuclear antigen (LANA) and LANA2 [1, 13, 14]. Although latent infection predominates in KSHV-infected PEL cell lines, phorbol ester stimulation can induce lytic infection in these cells [12]. Gene expression during the lytic phase is classified into immediate early, early, and late expression [12]. Open-reading frame (ORF)–50 was identified as an immediate early protein that was required for the lytic replication of KSHV [12, 15, 16]. Immunohistochemical studies demonstrated that KS cells expressed LANA; however, the expression of lytic proteins was very rare in KS lesions, which suggests that latent infection predominates in KS cells [5, 6, 17]. Lytic proteins are expressed by some B cells in the mantle zone of MCD, which suggests that lytic replication frequently occurs in MCD lesions [6, 17].

Numbers of KSHV copies in KSHV-associated diseases have been investigated by several groups [18–26]. An early study that used conventional PCR and South-

Received 10 August 2005; accepted 28 September 2005; electronically published 7 February 2006.

Financial support: Ministry of Health, Labor and Welfare (Health and Labor Sciences Research Grants on HIV/AIDS and Measures for Intractable Diseases H15-AIDS-005 to H.K. and 17243601 to T.S.); Ministry of Education, Culture, Sports, Science and Technology of Japan (Grant-in-Aid for Scientific Research 17590365 to H.K.); Japan Health Sciences Foundation (research grant on health sciences focusing on drug innovation SA14831 to H.K.).

Potential conflicts of interest: none reported.

Reprints or correspondence: Dr. Harutaka Katano, Dept. of Pathology, National Institute of Infectious Diseases, 1-23-1 Toyama, Shinjuku, Tokyo 162-8640, Japan (katano@nih.go.jp).

The Journal of Infectious Diseases 2006; 193:773–82

0022-1899/2006/19306-0006$15.00

Table 1. No. of copies of Kaposi sarcoma–associated herpesvirus (KSHV), determined by real-time polymerase chain reaction (PCR) and PCR–Southern blot.

	Real-time PCR		PCR–Southern blot	
Patient (disease)	Mean copies/cell	Average (SD)	No.	Mean copies/cell
1 (PEL)	82.01	82.01	1	50
2 (KSHV-associated solid lymphoma)	14.26	10.75 (4.97)	...	...
3 (KSHV-associated solid lymphoma)	7.23		2	2
4 (AIDS-associated patch KS)	0.09	0.13 (0.11)	...	...
5 (AIDS-associated plaque KS)	0.04		...	...
6 (AIDS-associated patch KS)	0.25		...	...
7 (AIDS-associated nodular KS)	0.67	1.72 (1.51)	3	2
8 (AIDS-associated nodular KS)	1.02		4	0.4
9 (AIDS-associated nodular KS)	0.53		...	...
10 (AIDS-associated nodular KS)	3.13		5	0.4
11 (AIDS-associated nodular KS)	3.93		6	2
12 (AIDS-associated nodular KS)	0.14		...	...
13 (AIDS-associated nodular KS)	3.41		...	...
14 (AIDS-associated nodular KS)	0.91		...	...
15 (classic patch KS)	0.16	2.60 (2.70)	...	...
16 (classic patch KS)	5.50		7	0.08
17 (classic patch KS)	2.13		...	...
18 (classic nodular KS)	0.00	1.64 (2.63)	...	...
19 (classic nodular KS)	4.67		8	2
20 (classic nodular KS)	0.25		...	...
21 (MCD)	0.27	0.27	9	1
22 (control, BCBL-1)	78.01	87.08 (12.83)	...	...
23 (control, TY-1)	96.15		...	...

NOTE. MCD, multicentric Castleman disease; PEL, primary effusion lymphoma.

ern blot analysis demonstrated that a PEL cell contained ~50 copies of KSHV genome, whereas the KSHV genome was detected at a rate of ~1 viral copy/cell in KS lesions [18]. Recently, real-time PCR was used to detect KSHV, and several reports have described numbers of viral copies in peripheral blood mononuclear cells (PBMCs) derived from patients with KS [19–26]. Studies using real-time PCR have demonstrated that numbers of viral copies in PBMCs varied among diseases and disease stages [21–24]. However, to our knowledge, there has been no report that has compared numbers of viral copies in KS, PEL, or MCD lesions using real-time PCR. Therefore, the aim of the present study was to determine numbers of viral copies in lesions of KSHV-associated diseases using pathologic samples. Pathologic tissue samples—such as biopsy samples—frequently contain both virus-infected cells and noninfected cells. Thus, results from real-time PCR do not solely represent numbers of viral copies in virus-infected cells. To solve this problem, we combined real-time PCR with computerized-image analysis that allowed an assessment of numbers of virus-infected cells in immunostained sections. Using these methods, we identified numbers of both viral copies and virus-infected cells in appropriate sections. Thus, we obtained relatively accurate numbers of viral copies in histologic sections of KSHV-associated disease lesions.

PATIENTS, MATERIALS, AND METHODS

Patients and samples. All patients provided informed consent for specimens to be obtained. For PCR analysis, 21 clinical samples were collected (table 1). For immunohistochemical analysis, 27 histopathologic specimens from KSHV-infected patients (table 2) were collected from 1995 to 2004. All KS specimens were categorized into groups according to the clinical stage of KS (patch, plaque, or nodular) on the basis of clinical and histologic data. DNA extracted from 2 KSHV-positive cell lines (BCBL-1 and TY-1), a KSHV-negative Epstein-Barr virus–positive Burkitt lymphoma cell line (Raji), and human umbilical vascular endothelial cells (HUVECs) was used as a control for PCR studies [27, 28].

Preparation of DNA. DNA was extracted from fresh-frozen clinical materials or from formalin-fixed, paraffin-embedded tissue samples from 21 biopsies of KSHV-infected patients (table 1). For fresh-frozen materials, the DNeasy Tissue Kit (Qiagen) was used in accordance with the manufacturer's instructions. For the isolation of DNA from formalin-fixed, paraffin-embedded biopsy samples, 5-μm sections (n = 3–4) were deparaffinized with xylene, digested with proteinase K, and processed for phenol/chloroform extraction with sodium acetate/ethanol precipitation.

Table 2. Percentage of latency-associated nuclear antigen (LANA)– or open-reading frame (ORF)–50–positive cells in immunohistochemical analysis (IHC) with computerized-image analysis.

IHC, samples	Cases, no.	Minimum/maximum (average), %
LANA		
AIDS-associated patch/plaque KS	11	12/95 (48)
AIDS-associated nodular KS	4	28/72 (57)
AIDS-associated KS involving LN	2	28/31 (30)
AIDS-associated KS involving GI tract	2	6/7 (7)
Classic patch/plaque KS	2	25/47 (36)
MCD	4	5/21 (8)
KSHV-associated solid lymphoma	2	79/80 (80)
ORF50		
AIDS-associated patch/plaque KS	5	0
AIDS-associated nodular KS	4	0
Classic KS, patch/plaque	2	0
MCD	5	1/3 (2)
KSHV-associated solid lymphoma	2	0/5 (3)

NOTE. GI, gastrointestinal; KSHV, Kaposi sarcoma–associated herpesvirus; LN, lymph node; MCD, multicentric Castleman disease.

Real-time quantitative PCR. Amounts of KSHV DNA were determined by quantitative real-time (TaqMan) PCR using the ABI Prism 7900HT sequence detection system (Applied Biosystems), which amplified segments within the KSHV LANA gene (one of the latent proteins coded on ORF73). Sequences and usage parameters of primers and probes have been described elsewhere [19]. We also determined the amounts of human genomic DNA that were present in DNA extracted from each specimen. Primers and probes for the gene encoding human glyceraldehyde 3-phosphate dehydrogenase (GAPDH) were designed, using Primer Express software (Applied Biosystems), to obtain a 104-bp amplicon. Forward and reverse primer sequences were 5′-GCTCCCTCTTTCTTTGCAGCAAT-3′ and 5′-TACCATGAGTCCTTCCACGATAC-3′, respectively. The fluorogenic TaqMan probe was 5′-(FAM)TCCTGCACCACCAACTGCTTAGCACC(TAMRA)-3′. PCR amplification was performed in 25-μL reaction mixtures using QuantiTect probe PCR Master Mix (Qiagen), 0.4 μmol/L each primer, 0.2 μmol/L TaqMan probe, and 2 μL of isolated DNA. PCR conditions were 15 min at 95°C, followed by 45 cycles of 15 s at 94°C and 1 min at 60°C. Quantitative results were obtained by generating standard curves for pGEM-T plasmids (Promega) that contained each KSHV (ORF73) and cellular target (GAPDH) amplicon. The number of viral copies per cell was calculated by dividing the number of ORF73 copies by one-half of the number of GAPDH copies, because there are 2 alleles of GAPDH in each cell.

Detection of KSHV by semiquantitative PCR–Southern blotting analysis. Semiquantitative PCR–Southern blotting was performed to determine copy numbers of KSHV in DNA samples after PCR amplification of $KS330_{233}$ [11, 29]. The β-globin gene was simultaneously amplified as described elsewhere [11]. For PCR–Southern blot analysis, digoxygenin (DIG)–labeled $KS330_{233}$ and a 110-bp DNA fragment of the β-globin gene, whose sequences were confirmed by sequencing, were used as probes [11]. Procedures for Southern blot analysis and the detection of DIG were those of the manufacturer (Roche Diagnostic). Copy numbers of KSHV were determined by comparing results for $KS330_{233}$ and β-globin, on the basis of the information that each cell has 2 copies of the β-globin genome.

Histologic and immunohistochemical analyses. Serial sections were prepared and stained with hematoxylin-eosin (HE) for light microscopy or were subjected to immunohistochemical staining with antiserum against LANA or ORF50 proteins (lytic antigens) [4, 30]. Immunohistochemical staining was visualized using the avidin-streptavidin-peroxidase method with 3-3′diaminobenzidine as the chromogen, as described elsewhere [4, 30]. For double immunohistochemical staining of vascular endothelial cell growth factor receptor–3 (VEGFR-3) and LANA, an anti-LANA rabbit polyclonal antibody, a peroxidase-conjugated anti-rabbit goat antibody (Envision; Dako Cytomation), and aminoethylcarbazole (AEC; Nichirei) were used as the primary antibody, secondary antibody, and chromogen, respectively. After the color development of AEC, slides were washed with PBS and processed for VEGFR-3 staining. Anti–VEGFR-3 mouse monoclonal antibody (D2-40; Nichirei) and alkaline phosphatase–conjugated anti–mouse IgG goat antibody (Envision; Dako Cytomation) were used, and a positive signal was detected with Fast Blue BB (Sigma-Aldrich). Slides were mounted with a glycerol-based mounting solution.

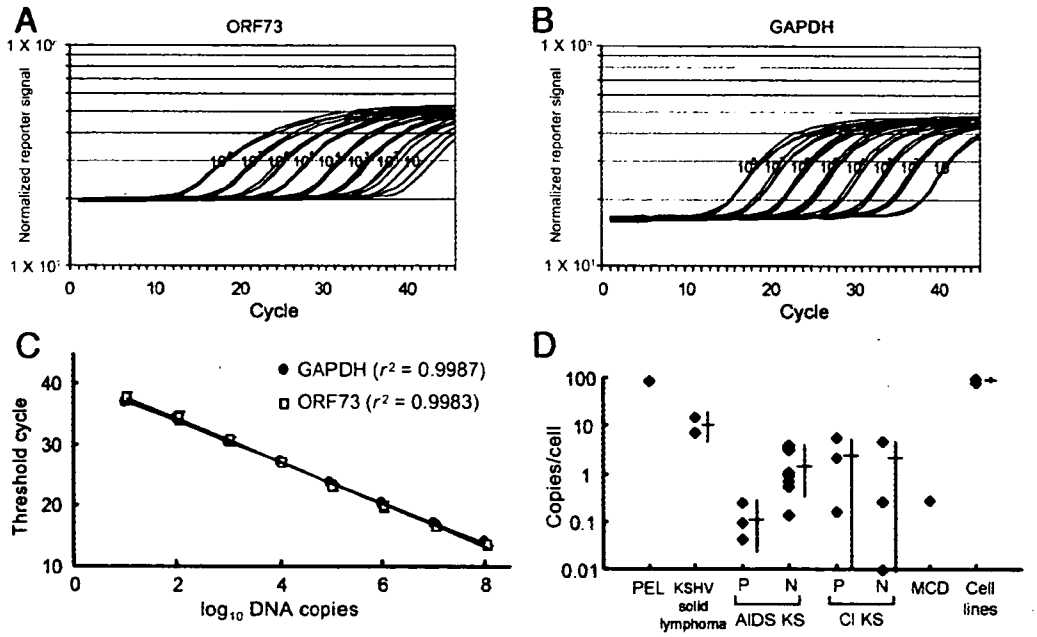

Figure 1. No. of copies of Kaposi sarcoma–associated herpesvirus (KSHV) in KSHV-associated diseases, determined by real-time polymerase chain reaction (PCR). *A* and *B*, Amplification curves of open-reading frame (ORF)–73 *(A)* and glyceraldehyde 3-phosphate dehydrogenase (GAPDH) genomes *(B)*. *C*, Standard curve of ORF73 and GAPDH genomes. *D*, No. of copies of KSHV per cell, calculated on the basis of the results of real-time PCR. Horizontal and vertical bars beside blots indicate average and SD, respectively. AIDS KS, AIDS-associated KS; Cl KS, classic KS; MCD, multicentric Castleman disease; N, nodular; P, patch; PEL, primary effusion lymphoma; Rn, normalized reporter signal.

Computerized-image analysis for KSHV-positive cells. To estimate numbers of KSHV-infected cells in lesions of KSHV-associated diseases, computerized analysis of immunohistochemical images was performed using ImageJ software (version 1.33u; National Institutes of Health). A representative image of each section from each sample was captured at ×40 or ×100 magnification. First, the image was split into red, green, and blue colors; then the 3 images were converted to gray-scale images. The total number of cells was counted in the red image, and the number of KSHV-infected cells (stained by the antiserum against KSHV proteins) was counted in the blue image. A threshold was set, for clear visualization of the displayed image. For counting cells, "analyze particle" was selected from "analyze" in the menu bar, and the minimum size was set at 30. After the accuracy of cell outlines generated by the software was verified, numbers of cells were calculated in separate windows.

RESULTS

Amount of KSHV viral genome in KSHV-associated lesions. To determine the relationships between amounts of KSHV genome and KSHV-associated diseases, we performed real-time PCR to detect KSHV ORF73 and GAPDH in appropriate DNA samples. Specificity of the assay for ORF73 was confirmed using a panel of DNA from other herpesviruses (HHV-1–7) and cellular DNA from HUVECs and Raji cells (data not shown). The assay for ORF73 uniformly detected 10 copies of pGEM-ORF73 plasmid (figure 1*A* and 1*C*). PCR amplification of GAPDH also uniformly detected 10 copies of GAPDH genome (figure 1*B* and 1*C*). Amplification plots and standard curves demonstrated a linear relationship between numbers of copies from 10 to 10^8 and the cycle threshold, which indicates that dynamic ranges of these 2 real-time PCRs were between 10 and 10^8 copies. To validate differences between DNA samples from frozen tissues and those from paraffin-embedded tissues, we tested a DNA sample from a frozen cell pellet of TY-1 and a DNA sample from a paraffin-embedded TY-1 cell pellet. No significant difference was detected between these 2 types of DNA (data not shown).

Results of real-time PCR showed signs of a positive association between the number of viral copies per cell and disease (table 1 and figure 1*D*). A DNA sample from PEL demonstrated a number of KSHV copies similar to that of PEL cell lines (PEL, 82; PEL cell lines, 87). DNA from samples of KSHV-associated solid lymphoma also showed a high number of KSHV copies (average, 10.8 viral copies/cell). DNA from samples of KS and MCD demonstrated lower numbers of viral copies than those of KSHV-associated lymphoma (PEL and KSHV-associated solid lymphoma). The average number of KSHV copies in DNA from KS samples was 1.58 viral copies/cell (range, 0.00–5.50

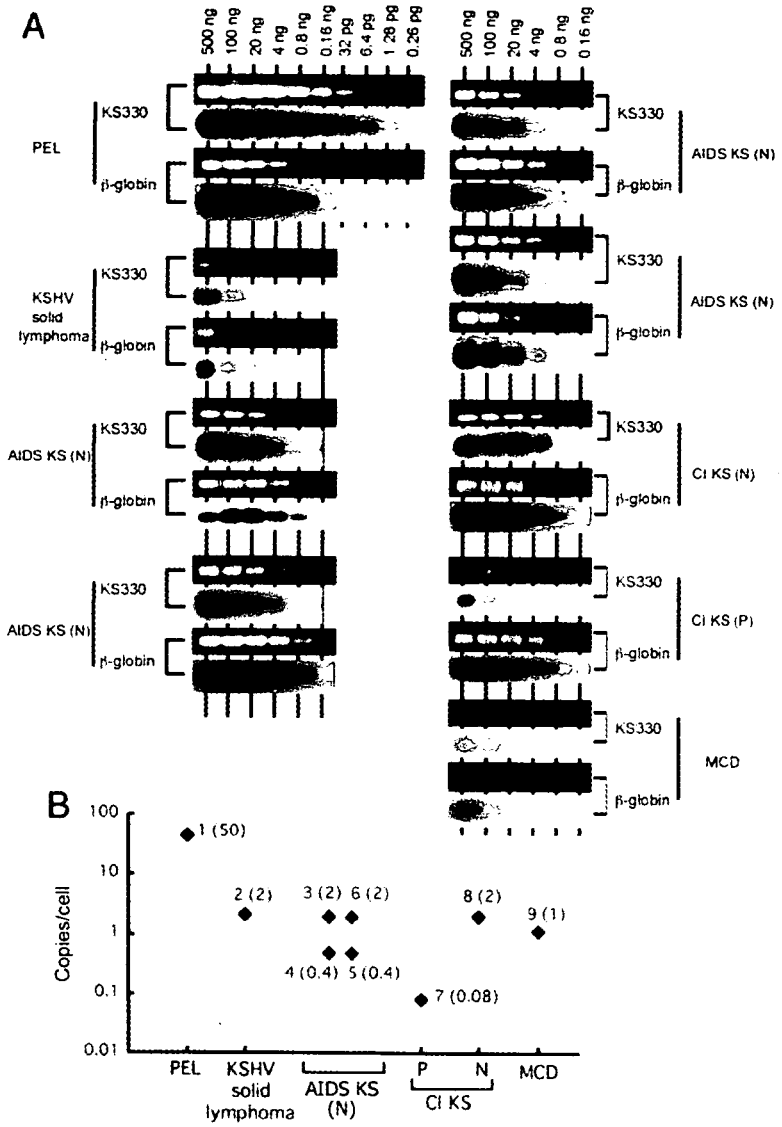

Figure 2. No. of copies of Kaposi sarcoma–associated herpesvirus (KSHV) in KSHV-associated disease, determined by conventional polymerase chain reaction (PCR)–Southern blotting. *A*, PCR–Southern blotting. DNA extracted from samples was serially diluted, and KS330 and β-globin genes were amplified from the diluted DNA. *Upper panels,* bands of PCR products in ethidium bromide–stained gel; *lower panels,* bands of products in PCR–Southern blots. *B,* No. of copies of KSHV in KSHV-associated diseases, determined by PCR–Southern blots. The nos. beside each dot correspond to the sample nos. in panel A. The nos. in parentheses indicate the nos. of viral copies per cell. AIDS KS, AIDS-associated KS; CI KS, classic KS; MCD, multicentric Castleman disease; N, nodular; P, patch.

viral copies/cell), whereas those in DNA samples from the nodular and patch/plaque stages of AIDS-associated KS samples were 1.72 and 0.13 viral copies/cell, respectively. DNA samples from classic KS (KS in patients without HIV infection) also had <5 viral copies/cell. A DNA sample from an MCD lesion had 0.27 viral copies/cell. To confirm these results, we performed semiquantitative PCR–Southern blot analysis using some of these samples. Results demonstrated similar copy numbers resulting from the 2 techniques (table 1 and figure 2). Thus, quantitative PCR analysis suggested that PEL might have the highest copy number (82 copies), followed by KSHV-associated solid lymphoma (11 copies). KS and MCD lesions contained lower copy numbers (~1 copy/cell), regardless of HIV-infection.

Number of KSHV-infected cells in KSHV-associated diseases. Because pathologic tissue samples present cells contaminated

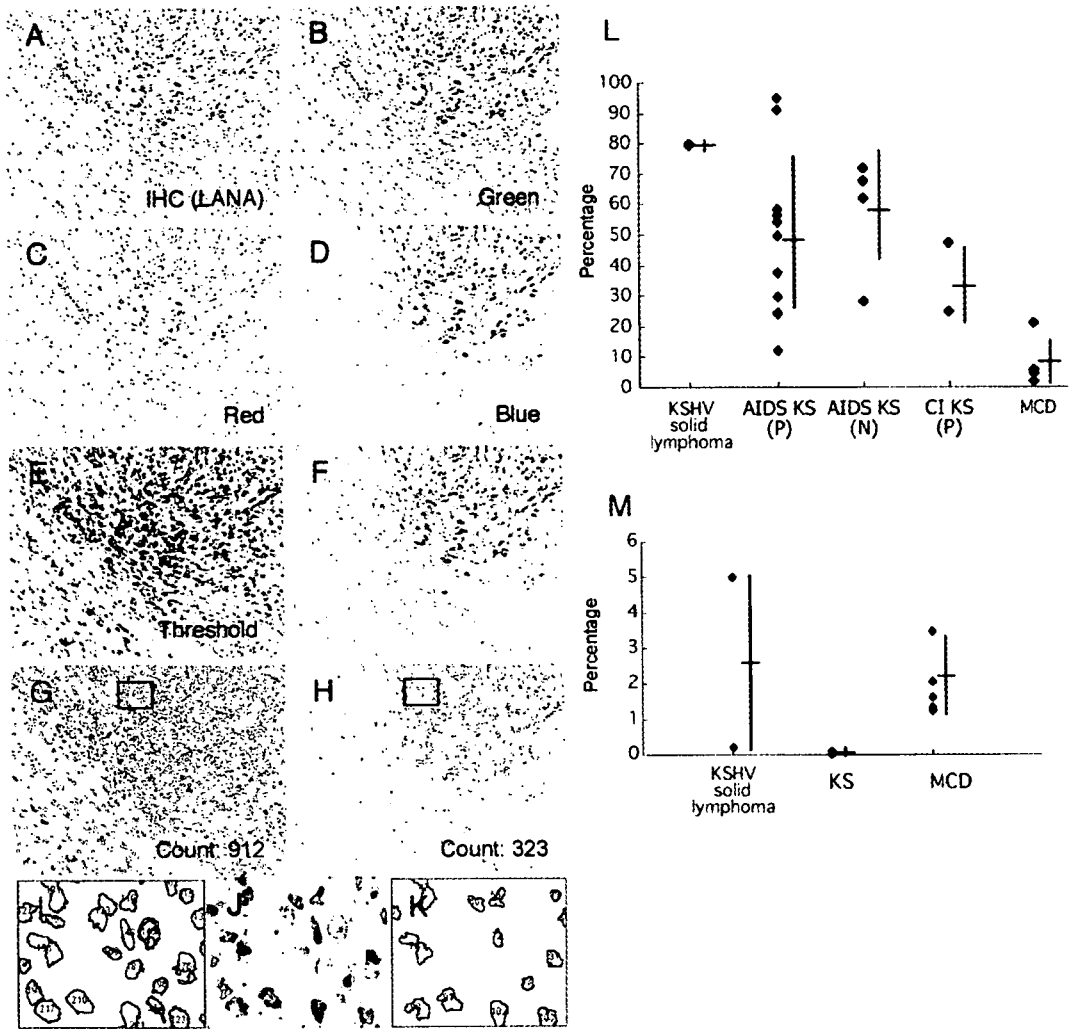

Figure 3. Computerized-image analysis of immunostaining. *A–K*, Samples of computerized-image analysis. *A*, Image of immunohistochemical analysis for latency-associated nuclear antigen (LANA) on the lymph node that Kaposi sarcoma (KS) cells infiltrate. *B–D*, Image separated in into red *(C)*, green *(B)*, and blue *(D)* splits. *E*, The threshold of all cells, determined on the basis of a red split. *F*, The threshold of positive cells, determined on the basis of a blue split. *G*, Tracing image of all cells. *H*, Tracing image of only positive cells. *I*, Enlarged image of a box from panel G. All cells were traced and counted. *J*, The image of immunohistochemical analysis corresponding to that in panel I. *K*, Enlarged image of a box in panel H. Only positive cells were traced and counted. *L*, Rate of LANA-positive cells in samples. Horizontal and vertical bars beside blots indicate the average and SD, respectively. *M*, Positive rate of open-reading frame (ORF)–50–positive cells. AIDS KS, AIDS-associated KS; CI KS, classic KS; KSHV, KS-associated herpesvirus; MCD, multicentric Castleman disease; N, nodular; P, patchy.

in varying degrees, all DNA samples that we used for real-time PCR actually contained DNA extracted from histologically normal cells and noninfected (LANA-negative) cells, as confirmed by histologic data. To determine accurate KSHV copy numbers in a KSHV-infected cell in a lesion, knowledge is required of accurate numbers of KSHV-infected cells in a specific sample. Thus, we performed computerized-image analysis of immunostained sections to estimate the number of KSHV-positive cells. Because it is recognized that all KSHV-infected cells express LANA in the nuclei, we counted cells expressing LANA in the nuclei as KSHV-infected cells. LANA was stained brown in immunohistochemical analysis, and cell nuclei were counterstained with hematoxylin (violet). Therefore, brown nuclei were counted as LANA-positive cells, and violet entities were counted as nuclei by the image-analysis software ImageJ (figure 3). Results revealed that 80% of cells in tissue samples from KSHV-associated solid lymphoma were LANA positive (table 2 and figure 3*L*). Tissues obtained from AIDS-associated and non–AIDS-associated KS contained 12%–95% (average, 49%) LANA-positive cells. The MCD sample contained 8% (range,

Table 3. No. of viral copies and percentage of latency-associated nuclear antigen (LANA–) or open-reading frame (ORF)–50–positive cells in Kaposi sarcoma–associated herpesvirus (KSHV)–associated diseases.

Samples	Detected viral copies/cell[a]	LANA positive,[b] %	ORF50 positive,[b] %	Lytic cells/ infected cells, %	Predicted viral copies/infected cell
PEL	82.01	ND	ND	ND	...
KSHV-associated solid lymphoma	10.7	80	3	4	13.4
KS	1.58	49	0	0	3.22
AIDS-associated KS	1.28	51	0	0	2.50
Patch/plaque	0.13	48	0	0	0.27
Nodular	1.72	57	0	0	3.02
Classic KS	2.12	36	0	0	5.89
MCD	0.27	8	2	25	3.38

NOTE. MCD, multicentric Castleman disease; ND, not done; PEL, primary effusion lymphoma.

[a] TaqMan polymerase chain reaction.

[b] Immunohistochemical analysis.

5%–21%) LANA-positive cells. By comparing results from quantitative PCR and computerized-image analysis, we predicted numbers of KSHV copies in virus-infected cells from KSHV-associated disease samples (table 3). The predicted number of KSHV copies was 3.2 viral copies/cell in KS lesions. We also counted cells positive for ORF50 protein, a lytic antigen encoded by KSHV (table 2 and figure 3*M*). There were 3% ORF50 protein–positive cells in KSHV solid lymphoma samples and even a smaller percentage in KS lesions (table 2 and figure 4). When we compared numbers of cells expressing ORF50 protein and those expressing LANA, it was clear that KS cells expressed LANA, but the expression of ORF50 protein was very rare in KS lesions (table 3). In MCD lesions, 2% of cells expressed ORF50 protein. Although only 8% of cells were virus infected in MCD lesions, 25% of virus-infected cells expressed ORF50 protein, which suggests the frequent lytic replication of KSHV in MCD. These data demonstrated that number of viral copies and positivity for LANA varied among KSHV-associated diseases, which suggests different mechanisms of viral pathogenesis.

Numbers of KSHV copies at each KS stage. KS lesions were categorized into 3 clinical stages: patch, plaque, and nodular. To determine the relationship between amounts of KSHV genome and KS clinical stage, amounts of viral genome and cellular gene present in DNA extracts from specimens at each KS stage were examined using quantitative real-time PCR (figure 1) and semiquantitative PCR–Southern blotting (figure 2). The number of KSHV copies was significantly lower in patch/plaque-stage lesions (range, 0.04–0.30 viral copies/cell; average, 0.13 viral copies/cell) than in nodular-stage lesions (range, 0.10–3.90 viral copies/cell; average, 1.72 viral copies/cell) ($P < .05$, Mann-Whitney U test). In contrast, the number of KSHV copies was similar in both patch/plaque- and nodular-stage lesions in classic KS. Computerized-image analysis of immunohistochemically stained sections revealed that LANA-positive cell populations in the nodular stage (57%) were larger than those in the patch/plaque stage (48%); however, there was no significant difference between them. Lytic ORF50 protein–positive cells were very rare (0%) in both stages (figure 3*L* and 3*M* and table 3), which implies that lesions in KS were mainly composed of proliferating KSHV latently infected cells. Differences in numbers of viral copies between the 2 stages in AIDS-associated KS may simply be related to the numbers of latently infected cells.

KSHV-positive cells during the early stage of KS. According to the results of quantitative PCR, relatively high numbers of KSHV copies were detected in patch-stage KS tissue samples (figure 1*D*). In addition, KSHV-positive cells were detected at a rate of ~50% even during the early stage of KS, although numbers of viral copies in DNA from patch-stage samples were lower than those in nodular-stage samples. To clarify why such a high number of viral copies was present during the patch stage of KS, we investigated the localization of KSHV-positive cells in histologically stained sections at the patch stage. Histologic analysis showed an abnormal enlargement of blood capillaries with extended endothelial cells during the patch stage (figure 4*A*). Spindle cells were also sometimes observed around vessels at this stage. Many previous research groups have reported that these spindle-shaped cells were positive for KSHV; however, there has been no report that has described the KSHV status of these extended endothelial cells in enlarged capillaries during the early stage of KS. Here, double labeling revealed that both enlarged endothelial cells and spindle cells around capillaries were positive for LANA and VEGFR-3 (figure 4*A* and 4*B*). VEGFR-3 is a marker of lymphatic endothelial cells, and it is known that KSHV infection alters the gene profile and induces the expression of VEGFR-3 in endothelial cells [31–33]. All KS spindle cells at every stage expressed both LANA and VEGFR-3 (figure 4*A*–4*F*). No signal for LANA or VEGFR-3 was found in normal endothelial cells from capillaries or blood vessels in KS lesions (figure 4*C* and 4*D*). These data suggest that KSHV may infect endothelial cells at a very early

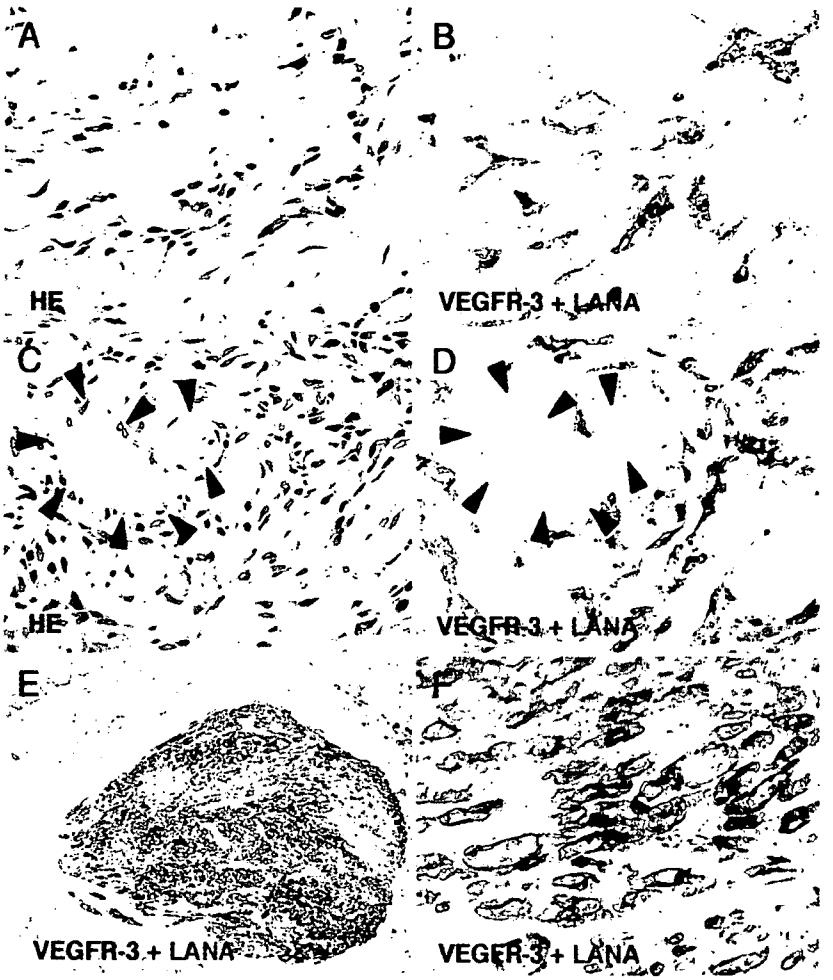

Figure 4. Kaposi sarcoma (KS)–associated herpesvirus–positive cells in various stages of KS. *A* and *B*, hematoxylin-eosin (HE) staining *(A)* and double immunohistochemical staining *(B)* of vascular endothelial cell growth factor receptor 3 (VEGFR-3) *(blue)* and latency-associated nuclear antigen (LANA) *(brown)* in serial sections of patch-stage KS. Original magnification, ×400. *C* and *D*, HE staining *(C)* and double immunohistochemical analysis *(D)* of VEGFR-3 *(blue)* and LANA *(red)* in serial sections of plaque-stage KS. Arrowheads indicate vascular endothelial cells. Original magnification, ×400. *E* and *F*, Double immunohistochemical analysis of VEGFR-3 *(blue)* and LANA *(red)* in nodular-stage KS. Original magnifications, ×100 *(E)* and ×400 *(F)*.

stage in KS lesions and that infection may induce an abnormal extension of endothelial cells and an enlargement of blood vessels, resulting in a relatively high number of KSHV copies.

DISCUSSION

In the present study, we evaluated numbers of viral copies and numbers of KSHV-infected cells in KSHV-associated diseases using real-time quantitative PCR and a computerized-image analytical method. The predicted number of KSHV copies was 3.2 viral copies/cell. The expression of ORF50 protein was rare or nonexistent in KS lesions, which suggests that latently infected cells were proliferating in KS lesions. In MCD samples, 25% of KSHV-infected cells expressed ORF50 protein, which implies that the lytic replication of KSHV was frequent in MCD lesions. To our knowledge, this is the first study describing both numbers of viral copies and numbers of virus-infected cells in pathologic samples from KSHV-associated disease lesions.

The combination of real-time PCR and computerized-image analysis allowed the prediction of numbers of viral copies per infected cell in each KSHV-associated disease. Predicted copy numbers per infected cell are listed in table 3. KS lesions might contain 0.27–5.89 viral copies/cell (average, 3.22 viral copies/cell) of KSHV. KSHV-associated solid lymphoma cells might contain >10 viral copies/cell. These numbers were close to the ones reported for KS cells (1 viral copy/cell) and PEL cells (50 viral copies/cell) [18, 19]. Because almost all KS cells express

LANA, a KS cell should have >1 copy of the virus. One molecule of LANA binds to 1 copy of the KSHV genome on chromosomes of host cells [34]. Immunohistochemical staining produces several dots of LANA in the nucleus of every KS cell [4, 6]. Thus, it is not surprising that a KS cell has several copies of KSHV. Like KS cells, PEL and KSHV-associated solid lymphoma cells exhibited several dots of LANA staining in their nucleus by immunohistochemical analysis, which suggests that PEL and KSHV-associated solid lymphoma cells also have several copies per cell. However, numbers of viral copies in PEL and KSHV-associated solid lymphoma cells were obviously higher than those in KS cells. One reason for that was that 3% of KSHV-associated solid lymphoma cells expressed ORF50 protein, which implies that a small population of lymphoma cells was in the lytic phase, whereas cells expressing ORF50 protein were very rare (<0.1%) in KS cells (table 3). These data suggest that there might be different systems involved in the maintenance or replication of viruses between KSHV-infected lymphoma cells and KS cells. KSHV-positive cells contained 3.38 viral copies/cell in MCD. This number seemed to be lower than what we expected, given that one-fourth of KSHV-infected cells expressed ORF50 protein. We could not determine numbers of viral copies in MCD, because numbers of viral copies might vary among cases, and we examined the virus titer in only one MCD sample. Further studies are definitely required to determine numbers of viral copies in MCD.

Our double immunohistochemical analysis revealed that flat endothelial cells of atypical vessels in early KS lesions expressed both LANA and VEGFR-3. It was difficult to distinguish KS cells from non-KS endothelial cells strictly in HE-stained sections of early KS lesions. VEGFR-3 is a useful marker for KS cells [33]. Our data suggest that a large proportion of extended endothelial cells in the patch stage of KS and KS spindle cells were already infected with KSHV. Because lytic protein expression was also rare during the patch stage, KSHV infected these cells latently. Thus, KSHV infection may be established in endothelial cells at a very early stage in KS lesions. We suggest that this is one of the reasons why numbers of KSHV copies in patch-stage lesions were similar to those in nodular-stage lesions of classic KS in real-time PCR results (figure 3).

Computerized-image analysis has been used by several groups to count cells in immunohistochemically stained sections [35–37]. Technically, our image analysis method was much easier than previously reported ones, in that (1) image files did not need to be captured at high magnification—relatively low magnifications (×40–×100, not ×400) are preferred; (2) splitting of images to red, green, and blue and counting of cells were done automatically; (3) tracing positive and negative cells could be easily visually confirmed; (4) it took only a few minutes to analyze an image; and (5) ImageJ is freeware. The unique features of the present study involve the combination of real-time PCR and computerized-image analysis. Real-time PCR is a powerful tool for measuring numbers of viral copies quickly and easily. However, every pathologic sample contains various numbers of normal cells, and it is impossible to extract DNA strictly from lesions in pathologic samples. Therefore, when DNA is extracted from pathologic samples that contain virus-infected cells, extracted DNA will contain not only DNA from virus-infected cells but also DNA from uninfected cells. Almost all studies that use real-time PCR encounter this limitation. Immunohistochemical analysis and in situ hybridization (ISH) are useful techniques that allow the localization of virus-infected cells. However, immunohistochemical analysis and ISH are not quantitative. Indeed, signal intensity does not correlate with copy number of the molecules or nucleotides, because signal intensity in immunohistochemical analysis and ISH differs among experiments and slides and depends on the conditions of staining or hybridization, such as incubation time, washing, temperature, fixation, and buffer. By combining real-time PCR and computerized-image analysis, the determination of relatively accurate virus numbers in infected cells becomes possible. Numbers of viral copies can be measured using real-time PCR, and numbers of virus-infected cells can be estimated with computerized-image analysis. Both results are required to assess numbers of viral copies in a virus-infected cell. In the present study, we analyzed 1 or a few pictures per slide using computerized-image analysis. Examination of a whole slide would be ideal; however, it is difficult to scan a whole slide using a high-resolution objective lens, but that may be available in the near future using, for example, a virtual slide system. In conclusion, the combination of real-time PCR and computerized-image analysis provides a useful tool for the prediction of numbers of viral copies in virus-associated diseases and of numbers of copies of certain molecules in a cell.

References

1. Moore PS, Chang Y. Kaposi's sarcoma-associated herpesvirus. In: Knipe DM, Howley PM, eds. Fields virology. Vol 2, 4th ed. Philadelphia: Lippincott, Williams & Wilkins, **2001**:2803–33.
2. Moore PS, Chang Y. Detection of herpesvirus-like DNA sequences in Kaposi's sarcoma in patients with and without HIV infection. N Engl J Med **1995**;332:1181–5.
3. Dupin N, Grandadam M, Calvez V, et al. Herpesvirus-like DNA sequences in patients with Mediterranean Kaposi's sarcoma. Lancet **1995**;345:761–2.
4. Katano H, Sato Y, Kurata T, Mori S, Sata T. High expression of HHV-8-encoded ORF73 protein in spindle-shaped cells of Kaposi's sarcoma. Am J Pathol **1999**;155:47–52.
5. Dupin N, Fisher C, Kellam P, et al. Distribution of human herpesvirus-8 latently infected cells in Kaposi's sarcoma, multicentric Castleman's disease, and primary effusion lymphoma. Proc Natl Acad Sci USA **1999**;96:4546–51.
6. Parravicini C, Chandran B, Corbellino M, et al. Differential viral protein expression in Kaposi's sarcoma-associated herpesvirus-infected diseases: Kaposi's sarcoma, primary effusion lymphoma, and multicentric Castleman's disease. Am J Pathol **2000**;156:743–9.
7. Nador RG, Cesarman E, Chadburn A, et al. Primary effusion lym-

phoma: a distinct clinicopathologic entity associated with the Kaposi's sarcoma-associated herpes virus. Blood **1996**; 88:645–56.
8. Katano H, Suda T, Morishita Y, et al. Human herpesvirus 8-associated solid lymphomas that occur in AIDS patients take anaplastic large cell morphology. Mod Pathol **2000**; 13:77–85.
9. Chadburn A, Hyjek E, Mathew S, Cesarman E, Said J, Knowles DM. KSHV-positive solid lymphomas represent an extra-cavitary variant of primary effusion lymphoma. Am J Surg Pathol **2004**; 28:1401–16.
10. Soulier J, Grollet L, Oksenhendler E, et al. Kaposi's sarcoma-associated herpesvirus-like DNA sequences in multicentric Castleman's disease. Blood **1995**; 86:1276–80.
11. Suda T, Katano H, Delsol G, et al. HHV-8 infection status of AIDS-unrelated and AIDS-associated multicentric Castleman's disease. Pathol Int **2001**; 51:671–9.
12. Sun R, Lin SF, Staskus K, et al. Kinetics of Kaposi's sarcoma-associated herpesvirus gene expression. J Virol **1999**; 73:2232–42.
13. Rivas C, Thlick AE, Parravicini C, Moore PS, Chang Y. Kaposi's sarcoma-associated herpesvirus LANA2 is a B-cell-specific latent viral protein that inhibits p53. J Virol **2001**; 75:429–38.
14. Rainbow L, Platt GM, Simpson GR, et al. The 222- to 234-kilodalton latent nuclear protein (LNA) of Kaposi's sarcoma-associated herpesvirus (human herpesvirus 8) is encoded by orf73 and is a component of the latency-associated nuclear antigen. J Virol **1997**; 71:5915–21.
15. Lukac DM, Kirshner JR, Ganem D. Transcriptional activation by the product of open reading frame 50 of Kaposi's sarcoma-associated herpesvirus is required for lytic viral reactivation in B cells. J Virol **1999**; 73: 9348–61.
16. Zhu FX, Cusano T, Yuan Y. Identification of the immediate-early transcripts of Kaposi's sarcoma-associated herpesvirus. J Virol **1999**; 73: 5556–67.
17. Katano H, Sato Y, Kurata T, Mori S, Sata T. Expression and localization of human herpesvirus 8-encoded proteins in primary effusion lymphoma, Kaposi's sarcoma, and multicentric Castleman's disease. Virology **2000**; 269:335–44.
18. Cesarman E, Chang Y, Moore PS, Said JW, Knowles DM. Kaposi's sarcoma-associated herpesvirus-like DNA sequences in AIDS-related body-cavity-based lymphomas. N Engl J Med **1995**; 332:1186–91.
19. Lallemand F, Desire N, Rozenbaum W, Nicolas JC, Marechal V. Quantitative analysis of human herpesvirus 8 viral load using a real-time PCR assay. J Clin Microbiol **2000**; 38:1404–8.
20. White IE, Campbell TB. Quantitation of cell-free and cell-associated Kaposi's sarcoma-associated herpesvirus DNA by real-time PCR. J Clin Microbiol **2000**; 38:1992–5.
21. Campbell TB, Borok M, Gwanzura L, et al. Relationship of human herpesvirus 8 peripheral blood virus load and Kaposi's sarcoma clinical stage. AIDS **2000**; 14:2109–16.
22. Tedeschi R, Enbom M, Bidoli E, Linde A, De Paoli P, Dillner J. Viral load of human herpesvirus 8 in peripheral blood of human immunodeficiency virus-infected patients with Kaposi's sarcoma. J Clin Microbiol **2001**; 39:4269–73.
23. Quinlivan EB, Zhang C, Stewart PW, Komoltri C, Davis MG, Wehbie RS. Elevated virus loads of Kaposi's sarcoma–associated human herpesvirus 8 predict Kaposi's sarcoma disease progression, but elevated levels of human immunodeficiency virus type 1 do not. J Infect Dis **2002**; 185:1736–44.
24. Boivin G, Cote S, Cloutier N, Abed Y, Maguigad M, Routy JP. Quantification of human herpesvirus 8 by real-time PCR in blood fractions of AIDS patients with Kaposi's sarcoma and multicentric Castleman's disease. J Med Virol **2002**; 68:399–403.
25. Engels EA, Biggar RJ, Marshall VA, et al. Detection and quantification of Kaposi's sarcoma-associated herpesvirus to predict AIDS-associated Kaposi's sarcoma. AIDS **2003**; 17:1847–51.
26. Song J, Yoshida A, Yamamoto Y, et al. Viral load of human herpesvirus 8 (HHV-8) in the circulatory blood cells correlates with clinical progression in a patient with HHV-8-associated solid lymphoma with AIDS-associated Kaposi's sarcoma. Leuk Lymphoma **2004**; 45:2343–7.
27. Renne R, Zhong W, Herndier B, et al. Lytic growth of Kaposi's sarcoma-associated herpesvirus (human herpesvirus 8) in culture. Nat Med **1996**; 2:342–6.
28. Katano H, Hoshino Y, Morishita Y, et al. Establishing and characterizing a CD30-positive cell line harboring HHV-8 from a primary effusion lymphoma. J Med Virol **1999**; 58:394–401.
29. Chang Y, Cesarman E, Pessin MS, et al. Identification of herpesvirus-like DNA sequences in AIDS-associated Kaposi's sarcoma. Science **1994**; 266:1865–9.
30. Katano H, Sato Y, Itoh H, Sata T. Expression of human herpesvirus 8 (HHV-8)-encoded immediate early protein, open reading frame 50, in HHV-8-associated diseases. J Hum Virol **2001**; 4:96–102.
31. Hong YK, Foreman K, Shin JW, et al. Lymphatic reprogramming of blood vascular endothelium by Kaposi sarcoma-associated herpesvirus. Nat Genet **2004**; 36:683–5.
32. Wang HW, Trotter MW, Lagos D, et al. Kaposi sarcoma herpesvirus-induced cellular reprogramming contributes to the lymphatic endothelial gene expression in Kaposi sarcoma. Nat Genet **2004**; 36:687–93.
33. Weninger W, Partanen TA, Breiteneder-Geleff S, et al. Expression of vascular endothelial growth factor receptor-3 and podoplanin suggests a lymphatic endothelial cell origin of Kaposi's sarcoma tumor cells. Lab Invest **1999**; 79:243–51.
34. Ballestas ME, Chatis PA, Kaye KM. Efficient persistence of extrachromosomal KSHV DNA mediated by latency-associated nuclear antigen. Science **1999**; 284:641–4.
35. Chantrain CF, DeClerck YA, Groshen S, McNamara G. Computerized quantification of tissue vascularization using high-resolution slide scanning of whole tumor sections. J Histochem Cytochem **2003**; 51:151–8.
36. Johansson AC, Visse E, Widegren B, Sjogren HO, Siesjo P. Computerized image analysis as a tool to quantify infiltrating leukocytes: a comparison between high- and low-magnification images. J Histochem Cytochem **2001**; 49:1073–79.
37. Lehr HA, Mankoff DA, Corwin D, Santeusanio G, Gown AM. Application of photoshop-based image analysis to quantification of hormone receptor expression in breast cancer. J Histochem Cytochem **1997**; 45: 1559–65.

JOURNAL OF VIROLOGY, Feb. 2006, p. 1121–1129 Vol. 80, No. 3
0022-538X/06/$08.00+0 doi:10.1128/JVI.80.3.1121–1129.2006

A Methionine-Rich Domain Mediates CRM1-Dependent Nuclear Export Activity of Borna Disease Virus Phosphoprotein

Hideyuki Yanai,[1]‡ Takeshi Kobayashi,[1]†‡ Yohei Hayashi,[1] Yohei Watanabe,[1] Naohiro Ohtaki,[1] Guoqi Zhang,[1] Juan Carlos de la Torre,[2] Kazuyoshi Ikuta,[1] and Keizo Tomonaga[1]*

Department of Virology, Research Institute for Microbial Diseases (BIKEN), Osaka University, Suita, Osaka 565-0871, Japan,[1] and Department of Neuropharmacology, The Scripps Research Institute, La Jolla, California[2]

Received 9 July 2005/Accepted 3 November 2005

Borna disease virus (BDV) is a nonsegmented, negative-strand RNA virus that replicates and transcribes in the nucleus of infected cells. Recently, we have demonstrated that BDV phosphoprotein (P) can modulate its subcellular localization through binding to the protein X, which is encoded in the overlapping open reading frame (T. Kobayashi et al., J. Virol. 77:8099–8107, 2003). This observation suggested a unique strategy of intracellular trafficking of a viral protein that is essential for the formation of a functional BDV ribonucleoprotein (RNP). However, neither the mechanism nor the consequences of the cytoplasmic retention or nuclear export of BDV X-P complex have been elucidated. In this study, we show that BDV P contains a bona fide nuclear export signal (NES) and can actively shuttle between the nucleus and cytoplasm. A transient transfection analysis of cDNA clones that mimic the BDV bicistronic X/P mRNA revealed that the methionine-rich (MetR) domain of P is responsible for the X-dependent cytoplasmic localization of the protein complex. Mutational and functional analysis revealed that the methionine residues within the MetR domain are critical for the activity of the NES of P. Furthermore, leptomycin B or small interfering RNA for inhibition of CRM1 strongly suggested that a CRM1-dependent pathway mediates nuclear export of P. Fluorescence loss in photobleaching analysis confirmed the nucleocytoplasmic shuttling of P. Moreover, we revealed that the nuclear export of P is not involved in the inhibition of the polymerase activity by X in the BDV minireplicon system. Our results may provide a unique strategy for the nucleocytoplasmic transport of viral RNP, which could be critical for the formation of not only infectious virions in the cytoplasm but also a persistent viral state in the nucleus.

Riboviruses, whose RNA biosynthetic processes, replication, and transcription take place in the nucleus of the infected cell, need to control the directional transport of their genomes through nuclear pore complexes. Recent studies have revealed that viral proteins play central roles in the regulation of nucleocytoplasmic trafficking of viral nucleic acids (2, 24). For instance, the nucleocapsid (NP) and nonstructural (NS2/NEP) proteins of influenza A virus are required for nuclear import and export, respectively, of the viral ribonucleoprotein (RNP) complex (16–18). Likewise, the Rev protein of human immunodeficiency virus type 1 mediates the nuclear transport of unspliced or single-spliced viral transcripts (21). The nucleocytoplasmic transport of viral components is an active and energy-dependent process mediated by specific nuclear localization and export signals termed NLS and NES, respectively, which are present within cargo molecules (2, 7). The interaction between NLS or NES with nuclear transport receptors known as importin and exportin, respectively, regulates the direction in which cargo molecules are transported (7, 23). The signal-dependent translocation of cargo molecules most likely contributes to the nucleocytoplasmic transport of viral components in infected cells, but the detailed mechanisms by which viruses control the directional transport of their genome-protein complexes remain poorly understood.

Borna disease virus (BDV) is an enveloped virus with a nonsegmented, negative-strand RNA genome that has a gene organization characteristic of mononegaviruses (MNV). However, based on its unique genetic and biological features, BDV is considered to be the prototypic member of a new virus family, *Bornaviridae*, within the order *Mononegavirales* (4, 5, 30). BDV is highly neurotropic and noncytopathic, and it appears to be exquisitely adapted to establish persistent infections (5, 30). BDV has the property, unique among known animal MNV, of a nuclear site for the replication and transcription of its genome. Therefore, the nucleocytoplasmic transport of BDV macromolecules plays a key role in the virus life cycle.

Recent studies have revealed that several BDV proteins including the nucleoprotein (N), phosphoprotein (P), and protein X (also called p10) contribute to the nucleocytoplasmic transport of BDV (8, 9, 28, 31, 34). Two isoforms of the BDV N (p40N and p38N) are found in BDV-infected cells. Whether p40N and p38N are encoded by two different mRNA species (22) or the usage of a second in-frame initiation AUG codon located 13 amino acids (aa) downstream in the BDV N open reading frame remains unsolved. Basic amino acid- and leucine-rich motifs present within BDV N have been shown to function as NLS and NES, respectively (8, 9). The function of

* Corresponding author. Mailing address: Department of Virology, Research Institute for Microbial Diseases, Osaka University, 3-1 Yamadaoka, Suita, Osaka 565-0871, Japan. Phone: 81 6 6879 8308. Fax: 81 6 6879 8310. E-mail: tomonaga@biken.osaka-u.ac.jp.

† Present Address: Department of Microbiology and Immunology, Vanderbilt University Medical Center, D-7235 Medical Center North Nashville, TN 37232-2581.

‡ H.Y. and T. K. contributed equally to this work.

the NES of N is mediated through the chromosome region maintenance protein 1 (CRM1)-dependent pathway (9). The NLS of N has been mapped to the 13 N-terminal amino acid residues, and therefore the p38N isoform lacks an NLS signal (8). The significance of the NLS-lacking p38N has not been determined, but our previous findings suggest that p38N might facilitate the nuclear export of the viral RNPs by increasing the relative number of NESs in the N multimer (9). Moreover, we showed that P could counteract the nuclear export activity of p38N (9), which resulted in the nuclear retention of p40N. These findings support the involvement of p38N and P in the regulation of the trafficking of the viral RNPs in BDV-infected cells (2, 9).

We have reported that a P-X interaction might also contribute to the regulation of the nucleocytoplasmic transport of BDV components (10). BDV P contains a bipartite NLS (28), and P can directly bind to all other components of the viral RNP (26, 27). The intracellular localization of P is drastically influenced by its interaction with X (10). Synthesis of protein X starts within the same mRNA transcription unit as P, but 49 nucleotides upstream, and it overlaps, in a different frame, with the 71 N-terminal amino acids of P (3). Notably, P was efficiently retained in the cytoplasm of BDV-infected cells only when expression of X could be detected in the same cell. Conversely, expression of X was below detection levels in BDV-infected cells in which P exhibited predominantly a nuclear location. Recently, studies using a BDV minireplicon system have shown that X has a strong inhibitory effect on RNA synthesis mediated by the BDV polymerase (19, 25). This X inhibitory effect has been proposed to operate via X interaction with P (20). These results suggest that the control of the nucleocytoplasmic transport of P may play a key role in not only the regulation of BDV RNP trafficking but also the activity of the virus polymerase complex. Therefore, the elucidation of the mechanisms underlying the regulation of the nucleocytoplasmic transport of P can provide important information for a better understanding of the biology of BDV.

Here, we show that BDV P has nuclear export activity that is mediated by an NES contained within a methionine-rich (MetR) domain spanning amino acid residues 145 to 158 of P, which has been previously shown to be required also for P oligomerization. We document that P proteins with a mutated MetR domain accumulate in the nucleus in the presence of X. Moreover, we present evidence that the methionine (M) residues within the MetR domain are critical for the nuclear export activity of P, which operates via the CRM1 pathway. We also demonstrate that BDV P shuttles between the nucleus and cytoplasm and that X interaction with P favors the activity of the NES over the NLS present in P, which leads to a predominant cytoplasmic distribution of the X-P complex. Finally, we provide data supporting the view that BDV X may modulate the BDV polymerase activity via direct interaction with the polymerase complex rather than by altering of the subcellular distribution of P. Our findings illustrate the complexity of interactions underlying the regulation of the intracellular trafficking of the X-P complex, which may be critical for the regulation of both the viral polymerase activity and nucleocytoplasmic trafficking of BDV RNP.

MATERIALS AND METHODS

Cells. The OL cell line, derived from a human oligodendroglioma (1), was cultured in Dulbecco's modified Eagle's medium-high glucose (4.5%) supplemented with 10% fetal bovine serum, 100 U of penicillin G per ml, 100 μg of streptomycin per ml, and 4 mM glutamine. The 293T, HeLa, and NIH 3T3 cell lines were cultured in Dulbecco's modified Eagle's medium-low glucose (1.0%) supplemented with 10% fetal bovine serum.

Plasmid construction. Expression vectors encoding X/P-GFP (pgX/P; GFP is green fluorescent protein), P (pgP) and FLAG-tagged P (pcPF) have been previously described (10). Expression vectors pcPHA and pcXHA encoding hemagglutinin (HA)-tagged P and X BDV proteins, respectively, were generated by subcloning the P and X open reading frames, respectively, into the EcoRI and XhoI sites of plasmid pcDNA3 (Invitrogen, San Diego, CA). Plasmids expressing mutant forms of X/P-GFP and P-FLAG were generated from pgX/P and pcPF, respectively, using appropriate PCR procedures. To generate pgX/PNLS, the NLS located between aa 18 and 41 of P was PCR amplified and subcloned into the NotI and XhoI sites of pcDNA3 to yield pcNLS. Finally, a fragment containing X/P-GFP was subcloned into the EcoR I and NotI sites in pcNLS. Plasmids pCFN-βGal and pCFNrev-βGal were kindly provided by M. Dobbelstein (Philipps-Universität, Germany). Detailed information about the primers and PCR procedures used to generate these plasmids is available from the authors. Nucleotide sequences of the recombinant plasmids were confirmed by DNA sequencing.

Cell transfection and gene expression assays. Cells were seeded in 60-mm tissue culture plates or eight-well chamber slides (Lab-Tek Nunc Inc., Naperville, Ill.). After an overnight culture, cells were transfected with Lipofectamine 2000 (Invitrogen). Gene expression in transfected cells was examined 24 to 48 h later using one, or several, of the following procedures: (i) indirect immunofluorescence, (ii) GFP fluorescence, (iii) immunoprecipitation, and (iv) Western blotting.

Protein pull-down assay. Transfected cells were lysed in NP-40 lysis buffer as described previously (9). Proteins in the soluble fraction were immunoreacted for 2 h with an anti-FLAG antibody (Sigma-Aldrich, St. Louis, Mo.) at 4°C, and the precipitates were then recovered by incubation with protein G agarose beads (Santa Cruz Biotechnology, Inc., Santa Cruz, Calif.) for 24 h at 4°C. After a thorough washing, proteins bound to the agarose beads were separated by sodium dodecyl sulfate-polyacrylamide gel electrophoresis and analyzed by Western blotting with an anti-HA antibody (Sigma-Aldrich). The specific reactions were detected by an ECL Western blotting kit (Amersham Pharmacia Biotech, Uppsala, Sweden).

LMB treatment assay. Leptomycin B (LMB) was kindly provided by M. Yoshida (The University of Tokyo). At 48 h posttransfection, the medium was replaced with fresh medium containing LMB (20 ng/ml). The cells were incubated for 3 h in the presence of LMB. After the LMB treatment, the cells were fixed, and then the subcellular localization of GFP fusion proteins was visualized by epifluorescence.

Heterokaryon assay. Nucleocytoplasmic shuttling of P was examined using a heterokaryon assay. Transfected HeLa cells were seeded on eight-well chamber slides (Lab-Tek Nunc Inc.) together with an equal number of NIH 3T3 cells. Protein synthesis was blocked with 50 μg of cycloheximide per ml for 1 h prior to the fusion. The cells were washed in phosphate-buffered saline and fused by the addition of 50% (wt/wt) polyethylene glycol. After 2 min, the cells were washed in phosphate-buffered saline and were incubated in medium containing cycloheximide (50 μg/ml) for 3 h. After fusion, the cells were fixed and stained with Hoechst 33258 (Sigma-Aldrich) and anti-β-galactosidase (β-Gal) (GIBCO/BRL, Rockville, Md.).

RNA interference. Sequences of small interfering RNA (siRNA) for depletion of human CRM1 (siCRM1) were described previously (13, 15). Transfection of OL cells with siCRM1, nonsilencing negative control siRNA (QIAGEN K.K., Tokyo, Japan), or mock transfection (transfection reagents only) was performed in 12-well plates using Lipofectamine 2000 (Invitrogen) according to the manufacturer's protocol. Twenty-four hour after siCRM1 transfection, pGFP-PR1 or pgX/Pwt was transfected into the cells, and the cells were harvested at 48 h posttransfection and lysed. Then, Western blot analysis was performed using a rabbit polyclonal anti-CRM1 antibody (Santa Cruz Biotechnology) or a mouse monoclonal anti-β-actin antibody (Sigma-Aldrich).

FLIP analysis. OL cells transfected with P containing either a wild-type (Pwt) or mutated NES were used in fluorescence loss in photobleaching (FLIP) experiments with a Digital Eclipse Spectral Imaging Confocal Laser Microscope C1si (Nikon Co., Japan) using the 488-nm laser line of an Ar laser, 2-mW optical fiber output, and detection at 500 to 530 nm. Cells were bleached in a spot with